

AD-A058 398

AIR FORCE INST OF TECH WRIGHT-PATTERSON AFB OHIO
A STUDY OF SUPERCELL CLOUD TOP TEMPERATURE SIGNATURES FROM GOES--ETC(U)
MAR 78 P B MILLS
AFIT-CI-78-62

F/G 22/2

UNCLASSIFIED

NL

1 OF 1
AD
A058398



UNCLASSIFIED

SECURITY CLASSIFICATION OF THIS PAGE (When Data Entered)

14
AFIT

REPORT DOCUMENTATION PAGE

1

READ INSTRUCTIONS
BEFORE COMPLETING FORM

1. REPORT NUMBER

2. GOVT ACCESSION NO.

3. RECIPIENT'S CATALOG NUMBER

4. TITLE (and Subtitle)

5. TYPE OF REPORT & PERIOD COVERED

6 A Study of Supercell Cloud Top
Temperature Signatures From GOES Enhanced Infrared
Imagery.9 Master's
Thesis

7. AUTHOR(s)

10 Captain Peter B. Mills

LEVEL

6. PERFORMING ORG. REPORT NUMBER

8. CONTRACT OR GRANT NUMBER(s)

9. PERFORMING ORGANIZATION NAME AND ADDRESS

AFIT Student at the University of Utah,
Salt Lake City, UT10. PROGRAM ELEMENT, PROJECT, TASK
AREA & WORK UNIT NUMBERS

11. CONTROLLING OFFICE NAME AND ADDRESS

AFIT/CI
WPAFB OH 45433

12. REPORT DATE

11 Mar 1978

13. NUMBER OF PAGES

57 pages 12 73p.

14. MONITORING AGENCY NAME & ADDRESS (if different from Controlling Office)

15. SECURITY CLASS. (of this report)

Unclassified

15a. DECLASSIFICATION/DOWNGRADING
SCHEDULE

16. DISTRIBUTION STATEMENT (of this Report)

Approved for Public Release; Distribution Unlimited

17. DISTRIBUTION STATEMENT (of the abstract entered in Block 20, if different from Report)

18. SUPPLEMENTARY NOTES

JOSEPH P. HIPPS, Major, USAF
Director of Information, AFIT

AUG 15 1978

19. KEY WORDS (Continue on reverse side if necessary and identify by block number)

20. ABSTRACT (Continue on reverse side if necessary and identify by block number)

DDC
RECEIVED
SEP 11 1978
F

012200 Inc

DD FORM 1473

EDITION OF 1 NOV 65 IS OBSOLETE

78

UNCLASSIFIED
SECURITY CLASSIFICATION OF THIS PAGE (When Data Entered)

78-62T

A STUDY OF SUPERCELL CLOUD TOP TEMPERATURE
SIGNATURES FROM GOES ENHANCED INFRARED IMAGERY
FOR 15 April 1976

by

Peter Benton Mills

An abstract of a thesis submitted to the faculty of The
University of Utah in partial fulfillment of the
requirements for the degree of

Master of Science

Elford George Astling Chairman, Supervisory Committee
Department of Meteorology

~~Department of Meteorology~~

The University of Utah

March 1978

78 08 31 016

ACCESSION for	
NTIS	White Section
DDC	Buff Section
UNANNOUNCED	
JUSTIFICATION	
BY	
DISTRIBUTION/AVAILABILITY CODES	
Dist:	Avail. 001/01 SP.C
A	

ABSTRACT

GOES enhanced infrared imagery (10.5 to 12.5 μ m) was used to investigate overshooting tops on cirrus anvils for a severe weather situation that occurred on 15 April 1976 over the Midwest. Very interesting features of this imagery were small areas of relatively warm radiative temperatures imbedded within cold radiative temperature fields of large cirrus anvils. The location of these warm spots coincided with the radar location of tropopause penetrating tops from intense thunderstorms. Satellite infrared film loops, radar observations, and radiosonde reports were used to study the overshooting tops, while surface and upper air charts were used to study the synoptic scale features leading to convective storm development.

Models for the cloud dome of a vigorous, quasi-steady supercell storm are presented to explain the warm cloud top temperatures above the strong updraft region observed in enhanced infrared imagery. Features included in the model are (1) emissivity differences between the expanding cirrus anvil and the cloud dome center, (2) a mixing layer near the cloud top in which

78 08 31 016

moist ascending air is diluted with stratospheric air, and
(3) a vertical temperature profile with coldest air in the
cloud and a pronounced inversion at the cloud top.

A STUDY OF SUPERCELL CLOUD TOP TEMPERATURE
SIGNATURES FROM GOES ENHANCED INFRARED IMAGERY
FOR 15 APRIL 1976

by
Peter Benton Mills

A thesis submitted to the faculty of The
University of Utah in partial fulfillment of the
requirements for the degree of

Master of Science

Department of Meteorology
The University of Utah
March 1978

THE UNIVERSITY OF UTAH GRADUATE SCHOOL

SUPERVISORY COMMITTEE APPROVAL

of a thesis submitted by

Peter Benton Mills

I have read this thesis and have found it to be of satisfactory quality for a master's degree.

Feb 24, 1978

Date

Elford G. Astling

Elford G. Astling
Chairman, Supervisory Committee

I have read this thesis and have found it to be of satisfactory quality for a master's degree.

2/24/78

Date

Don R. Dickson

Don R. Dickson
Member, Supervisory Committee

I have read this thesis and have found it to be of satisfactory quality for a master's degree.

Feb 24, 1978

Date

Kuo-Nan Liou

Kuo-Nan Liou
Member, Supervisory Committee

THE UNIVERSITY OF UTAH GRADUATE SCHOOL

FINAL READING APPROVAL

To the Graduate Council of The University of Utah:

I have read the thesis of Peter Benton Mills in its final form and have found that (1) its format, citations, and bibliographic style are consistent and acceptable; (2) its illustrative materials including figures, tables, and charts are in place; and (3) the final manuscript is satisfactory to the Supervisory Committee and is ready for submission to the Graduate School.

February 27, 1978
Date

Elford G. Astling
Elford G. Astling
Member, Supervisory Committee

Approved for the Major Department

S. K. Kao
S. K. Kao
Chairman Dean

Approved for the Graduate Council

Dean of The Graduate School

ABSTRACT

GOES enhanced infrared imagery (10.5 to 12.5 μm) was used to investigate overshooting tops on cirrus anvils for a severe weather situation that occurred on 15 April 1976 over the Midwest. Very interesting features of this imagery were small areas of relatively warm radiative temperatures imbedded within cold radiative temperature fields of large cirrus anvils. The location of these warm spots coincided with the radar location of tropopause penetrating tops from intense thunderstorms. Satellite infrared film loops, radar observations, and radiosonde reports were used to study the overshooting tops, while surface and upper air charts were used to study the synoptic scale features leading to convective storm development.

Models for the cloud dome of a vigorous, quasi-steady supercell storm are presented to explain the warm cloud top temperatures above the strong updraft region observed in enhanced infrared imagery. Features included in the model are (1) emissivity differences between the expanding cirrus anvil and the cloud dome center, (2) a mixing layer near the cloud top in which

moist ascending air is diluted with stratospheric air, and (3) a vertical temperature profile with coldest air in the cloud and a pronounced inversion at the cloud top.

ACKNOWLEDGEMENTS

I would like to express my sincere thanks and appreciation to Dr. Elford Astling for all the guidance, time, and encouragement he gave me during the preparation of this thesis. Additionally, I want to thank Dr. Kuo-Nan Liou for his advice concerning the cloud top radiative transfer characteristics, and for serving along with Professor Don Dickson as committee members.

Special thanks go to my wife for her love and support throughout this investigation plus her typing of the manuscript.

Praise God for this special blessing. (John 14:6)

TABLE OF CONTENTS

ABSTRACT	iv
ACKNOWLEDGEMENTS	vi
LIST OF FIGURES	viii
CHAPTER	
I. INTRODUCTION	1
II. SYNOPTIC SITUATION	3
III. SATELLITE AND SATELLITE IMAGERY	25
IV. WARM INFRARED TEMPERATURE SIGNATURES	37
V. CLOUD TOP MODEL	44
VI. SUMMARY AND FURTHER STUDIES	55
REFERENCES	56
VITA	58

LIST OF FIGURES

	<u>Page</u>
Figure 1 Chart of 700 mb surface for 0000 GMT 13 April 1976; solid lines are contours (gpm) and dashed lines are isotherms (°C); surface frontal positions are superimposed	4
Figure 2 Chart of 700 mb surface for 0000 GMT 14 April 1976; solid lines are contours (gpm) and dashed lines are isotherms (°C); surface frontal position is superimposed	4
Figure 3 Chart of 700 mb surface for 1200 GMT 14 April 1976; solid lines are contours (gpm) and dashed lines are isotherms (°C); surface frontal position is superimposed	5
Figure 4 Chart of 700 mb surface for 0000 GMT 15 April 1976; solid lines are contours (gpm) and dashed lines are isotherms (°C); surface frontal position is superimposed	5
Figure 5 Chart of 700 mb surface for 1200 GMT 15 April 1976; solid lines are contours (gpm) and dashed lines are isotherms (°C); surface frontal positions are superimposed	6
Figure 6 Chart of 700 mb surface for 0000 GMT 16 April 1976; solid lines are contours (gpm) and dashed lines are isotherms (°C); surface frontal positions are superimposed	6
Figure 7 Chart of 200 mb surface for 0000 GMT 13 April 1976; solid lines are contours (gpm) and dashed lines are isotachs ($> 34 \text{ ms}^{-1}$)	9

	<u>Page</u>
Figure 8 Chart of 200 mb surface for 0000 GMT 14 April 1976; solid lines are contours (gpm) and dashed lines are isotachs ($> 34 \text{ ms}^{-1}$)	9
Figure 9 Chart of 200 mb surface for 1200 GMT 14 April 1976; solid lines are contours (gpm) and dashed lines are isotachs ($> 34 \text{ ms}^{-1}$)	10
Figure 10 Chart of 200 mb surface for 0000 GMT 15 April 1976; solid lines are contours (gpm) and dashed lines are isotachs ($> 34 \text{ ms}^{-1}$)	10
Figure 11 Chart of 200 mb surface for 1200 GMT 15 April 1976; solid lines are contours (gpm) and dashed lines are isotachs ($> 34 \text{ ms}^{-1}$)	11
Figure 12 Chart of 200 mb surface for 0000 GMT 16 April 1976; solid lines are contours (gpm) and dashed lines are isotachs ($> 34 \text{ ms}^{-1}$)	11
Figure 13 Chart of 850 mb relative humidity for 0000 GMT 13 April 1976; isopleths are in percent	15
Figure 14 Chart of 850 mb relative humidity for 0000 GMT 14 April 1976; isopleths are in percent	15
Figure 15 Chart of 850 mb relative humidity for 1200 GMT 14 April 1976; isopleths are in percent	16
Figure 16 Chart of 850 mb relative humidity for 0000 GMT 15 April 1976; isopleths are in percent	16
Figure 17 Chart of 850 mb relative humidity for 1200 GMT 15 April 1976; isopleths are in percent	17
Figure 18 Chart of 850 mb relative humidity for 0000 GMT 16 April 1976; isopleths are in percent	17

	<u>Page</u>
Figure 19 Chart of Showalter stability index for 0000 GMT 13 April 1976	20
Figure 20 Chart of Showalter stability index for 0000 GMT 14 April 1976	20
Figure 21 Chart of Showalter stability index for 1200 GMT 14 April 1976	21
Figure 22 Chart of Showalter stability index for 0000 GMT 15 April 1976	21
Figure 23 Chart of Showalter stability index for 1200 GMT 15 April 1976	22
Figure 24 Chart of Showalter stability index for 0000 GMT 16 April 1976	22
Figure 25 MB enhancement curve for GOES infrared data; abscissa is radi- ative temperature in °C and ordi- nate is the image gray scale	28
Figure 26 GOES MB enhanced infrared image of the central United States for 0732 GMT 15 April 1976	29
Figure 27 Radar summary of the central United States for 0735 GMT 15 April 1976	29
Figure 28 GOES MB enhanced infrared image of Iowa-Wisconsin area for 0532 GMT 15 April 1976	31
Figure 29 Radar summary of Iowa-Wisconsin area for 0535 GMT 15 April 1976	31
Figure 30 GOES MB enhanced infrared image of Iowa-Wisconsin area for 0632 GMT 15 April 1976	33
Figure 31 Radar summary of Iowa-Wisconsin area for 0635 GMT 15 April 1976	33
Figure 32 GOES MB enhanced infrared image of central United States for 2330 GMT 14 April 1976; grid 2 nm	34

	<u>Page</u>
Figure 33	GOES MB enhanced infrared image of central United States for 0130 GMT 15 April 1976; grid 1 nm 34
Figure 34	GOES infrared image of the central United States for 0730 GMT 15 April 1976 36
Figure 35	Path of warm spot of MB enhanced infrared images over Iowa from 0502 to 0732 GMT 15 April 1976; corresponding radar positions are shown also 39
Figure 36	Supercell cloud model with warm cloud dome; temperature, motion fields, and cloud emissivities are depicted 45
Figure 37	Infrared radiative temperature difference between the central cloud dome and various radial distances from the dome 48
Figure 38	Radiosonde data for Oklahoma City (left) and St. Cloud (right) 15 April 1976 50
Figure 39	Cloud dome model for central Iowa warm spot shown in Fig. 28; vertical lines A, B, C, and D represent se- lected columns the temperature, emissivity, and equivalent black body temperature of which are shown in Table 2 51
Figure 40	Model of a supercell with a cold cloud dome 54


CHAPTER I

INTRODUCTION

Infrared photographs from Geostationary Operational Environmental Satellites (GOES) have provided valuable information about cloud heights and mapping day and night cloud fields. High, thick cirrostratus clouds can be easily distinguished from low stratus clouds with infrared imagery while it may not always be possible with visible imagery alone. Life cycles of convective activity that are initiated during the daytime and continue after sunset can be investigated as demonstrated by Martin (1975). Moreover, infrared pictures can be enhanced by changing the gray scale over a limited temperature range, thereby retaining the information content of the data and delineating cloud features that may otherwise remain undetected (Corbell, et al., 1977).


→ This thesis investigated a case where enhanced infrared (EIR) imagery provided unique information about convective penetration above the tropopause for a severe weather situation over the central United States. This situation was unique because warm spots appeared over cumulonimbus tops in the GOES EIR imagery (Mills and

→ over



Astling, 1977). The warm spots corresponded to locations where radar observations indicated intense convection with tropopause penetrating tops had occurred. Generally, one would expect the overshooting tops to appear as cold areas in satellite infrared and enhanced infrared imagery because of moist adiabatic cooling in ascending convective motion.

Since GOES imagery is an important tool in severe local storm detection and prediction, and since enhancement of GOES data only became operational in early 1976, this investigation attempts to provide an explanation for the appearance of warm spots. Additionally, situations where warm spots did not occur are discussed.



CHAPTER II

SYNOPTIC SITUATION

On the afternoon and evening of 14 April 1976 (LST), severe thunderstorm activity developed over the Central states. The synoptic weather pattern was characterized by low level confluence in a frontal boundary with warm, moist southerly flow ahead of the front and dry westerly flow behind it. Diffluent, anticyclonic motion was present in the upper levels and provided favorable conditions for convective activity to develop within very unstable air near the frontal zone. In this chapter these synoptic features will be traced from the period 0000 GMT 13 April to 0000 GMT 16 April using the 700 and 200 mb charts, the 850 mb moisture field, and the Showalter stability index.

700 Millibar Winds and Surface Fronts

On 0000 GMT 13 April a stationary front extended from the Florida peninsula through the Gulf Coast states to a warm front over Texas as shown in Fig. 1. This frontal system was very weak and dissipated on the following days as a high pressure ridge developed over the Great Plains states. Evolution of these features is evident in Figs. 1 through 6 which show the surface

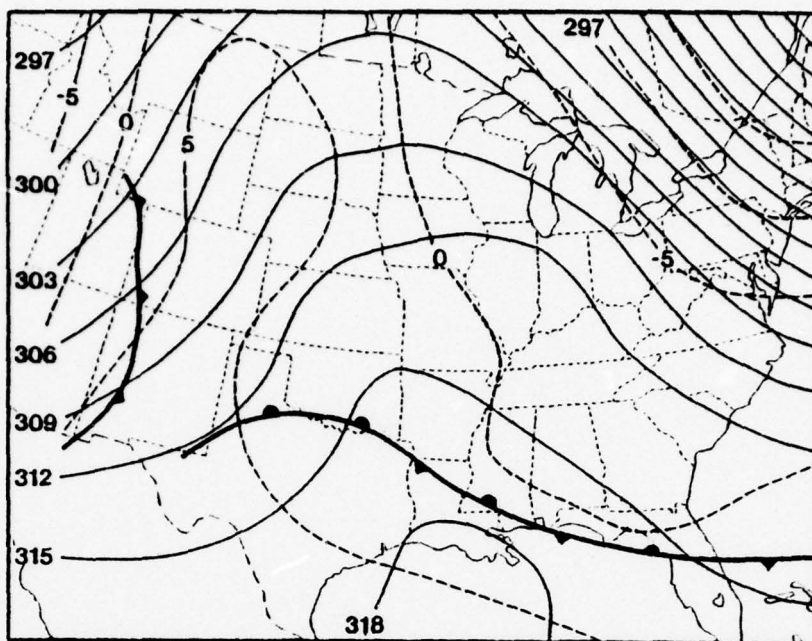


Figure 1 Chart of 700 mb surface for 0000 GMT 13 April 1976; solid lines are contours (gpm) and dashed lines are isotherms ($^{\circ}\text{C}$); surface frontal position are superimposed.

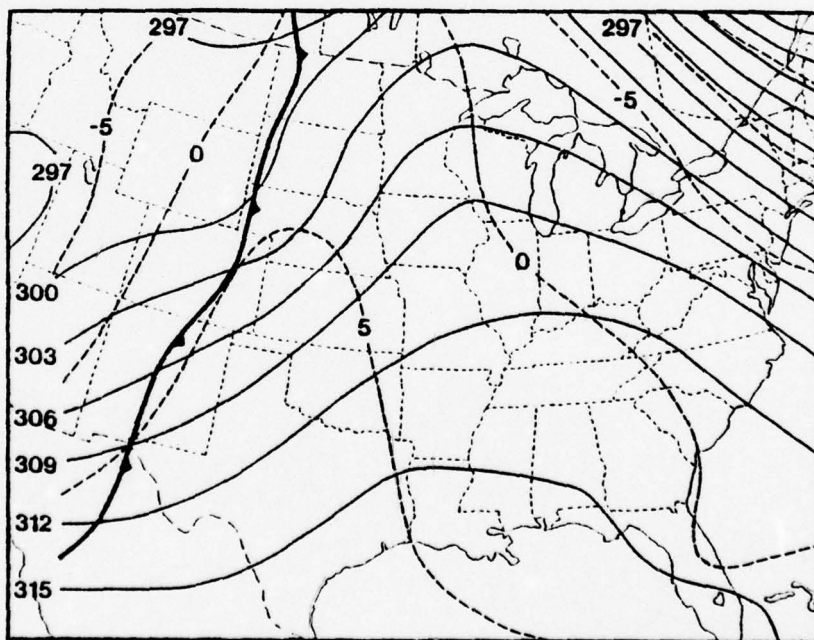


Figure 2 Chart of 700 mb surface for 0000 GMT 14 April 1976; solid lines are contours (gpm) and dashed lines are isotherms ($^{\circ}\text{C}$); surface frontal position is superimposed.

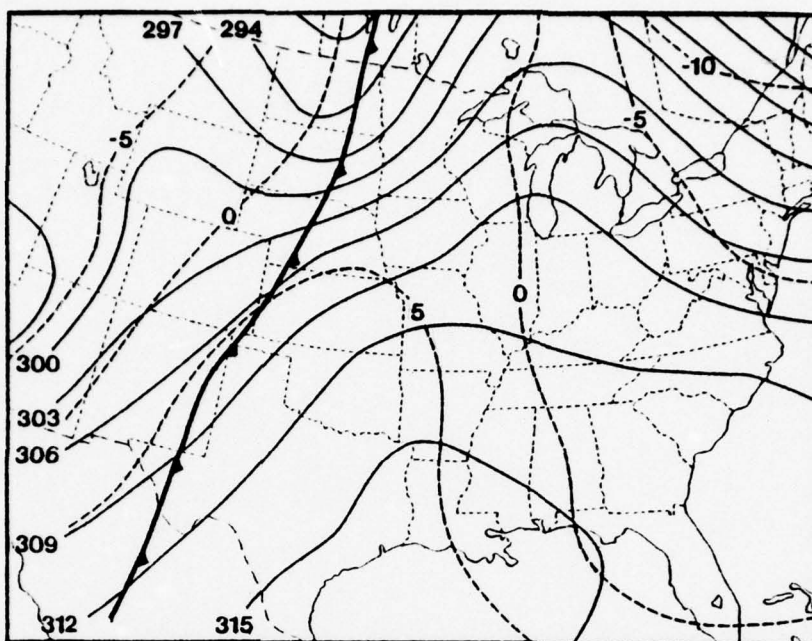


Figure 3 Chart of 700 mb surface for 1200 GMT 14 April 1976; solid lines are contours (gpm) and dashed lines are isotherms ($^{\circ}\text{C}$); surface frontal position is superimposed.

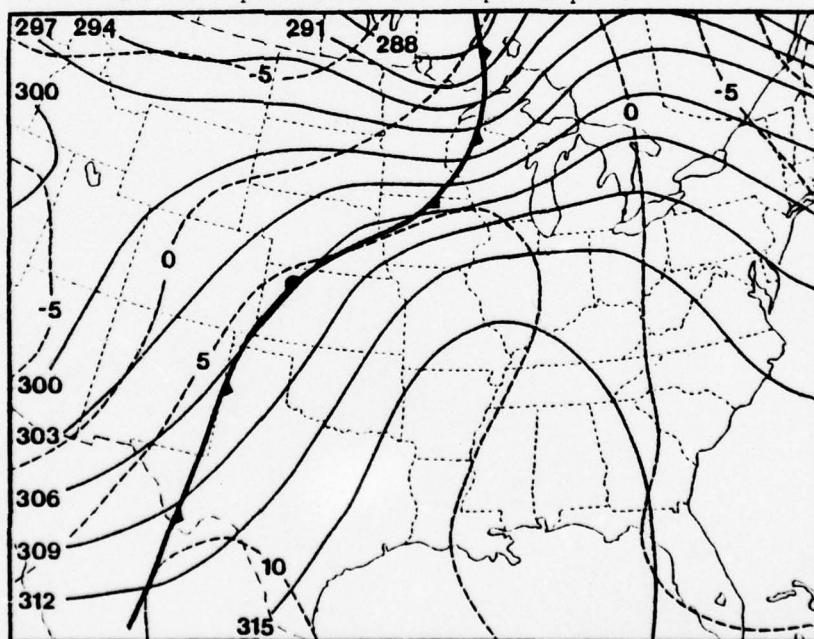


Figure 4 Chart of 700 mb surface for 0000 GMT 15 April 1976; solid lines are contours (gpm) and dashed lines are isotherms ($^{\circ}\text{C}$); surface frontal position is superimposed.

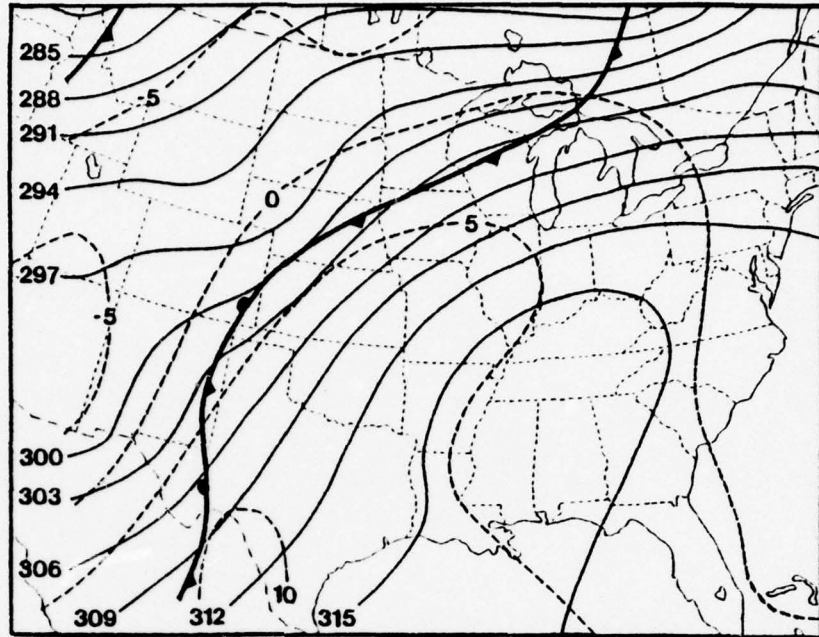


Figure 5 Chart of 700 mb surface for 1200 GMT 15 April 1976; solid lines are contours (gpm) and dashed lines are isotherms ($^{\circ}\text{C}$); surface frontal positions are superimposed.

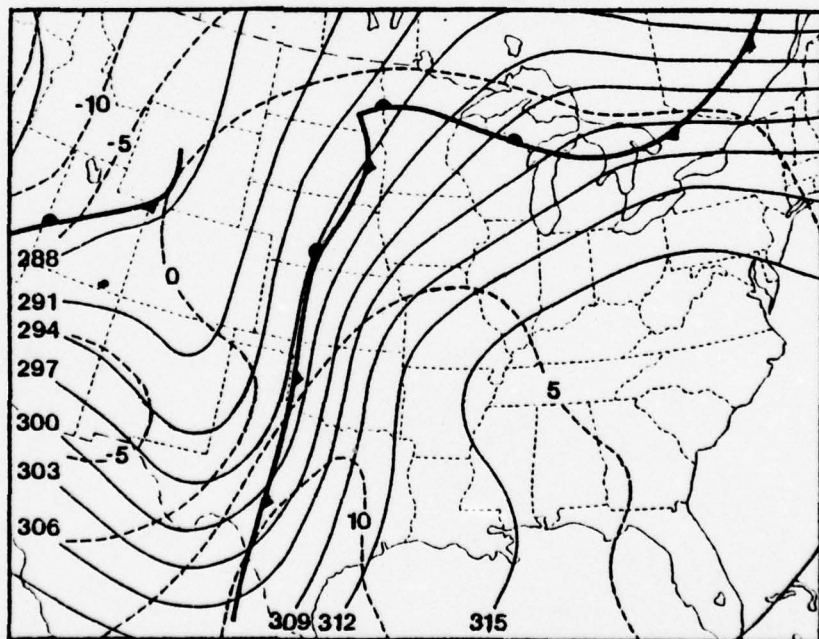


Figure 6 Chart of 700 mb surface for 0000 GMT 16 April 1976; solid lines are contours (gpm) and dashed lines are isotherms ($^{\circ}\text{C}$); surface frontal positions are superimposed.

frontal positions superimposed on the 700 mb charts of height and temperature fields. A low level ridge was well defined at 700 mb in Fig. 2 and extended northward from the Gulf of Mexico, across Louisiana and into the central United States. The entire ridge was moving eastward, as a trough over the western U.S. and an associated cold front were moving slowly eastward across Arizona and Utah into New Mexico and Colorado (Figs. 1 and 2). On 14 April a short wave trough moved rapidly eastward across the northern Great Plains and southern Canada. By 15 April the eastward moving cold front was located over the Great Lakes region and extended southward across the western Plains through eastern Colorado and into eastern New Mexico (Fig. 5). On 0000 GMT 14 April convective activity developed ahead of this frontal system in the northern Plain states. (A more detailed discussion of convective activity will accompany the atmospheric stability discussion.)

Within this period, the 700 mb ridge moved eastward into the Mississippi River Valley. Additionally, as the ridge moved eastward low level southerly flow advected moisture northward across the Central states. On 1200 GMT 14 April, however, pronounced warm air advection over Texas retarded the eastward ridge movement over the Gulf Coast states and this part of the ridge retrograded (Fig. 3). On the next day

this system began to move eastward again. During the period from 1200 GMT 14 April (Fig. 3) to 0000 GMT 15 April (Fig. 4), the cold front from southwest Texas through the central Plains continued to move very slowly eastward since the mid-level flow was parallel to the front.

In Fig. 4, confluent southerly flow was present over Texas while southwesterly flow prevailed ahead of the front further north. In addition to being confluent, the 700 mb flow was warm and now dry ahead of the frontal system (Figs. 2, 3, 4, and 5). This low level warm air advection helped increase the instability of the air mass over the Central states.

Intense convective activity continued through 15 April. Figs. 5 and 6 show the shift of the 700 mb wind flow and surface frontal position during this time.

200 Millibar Winds

In the upper levels at 0000 GMT 13 April (Fig. 7), relatively high wind speeds extended across the Southern and Eastern states. Figs. 7 through 12 show the 200 mb height field and isotach analysis. At 0000 GMT 13 April an extensive, eastward moving ridge covered the Central U.S. and Canada. A trough had moved inland over the West Coast. Between 0000 GMT 13 April and 0000 GMT 14 April, both the ridge and trough continued to move eastward.

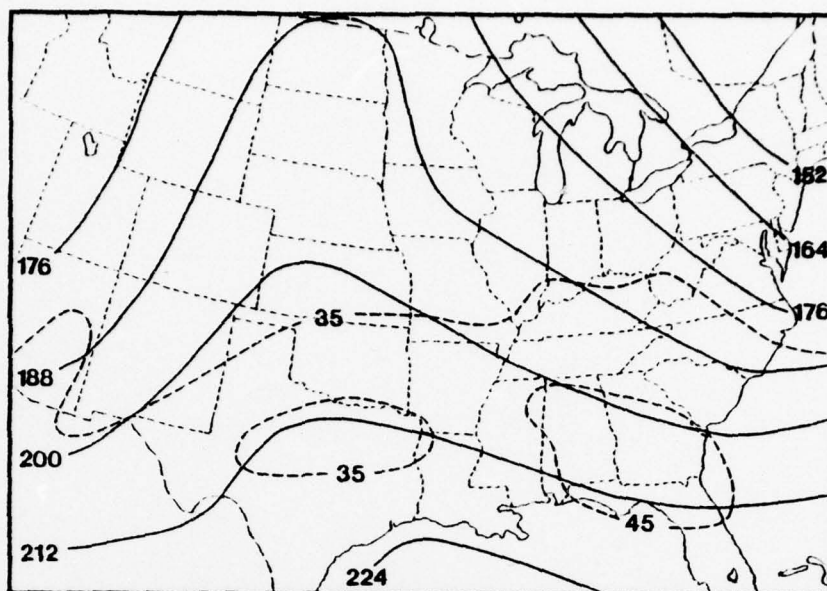


Figure 7 Chart of 200 mb surface for 0000 GMT 13 April 1976; solid lines are contours (gpm) and dashed lines are isotachs ($> 34 \text{ ms}^{-1}$).

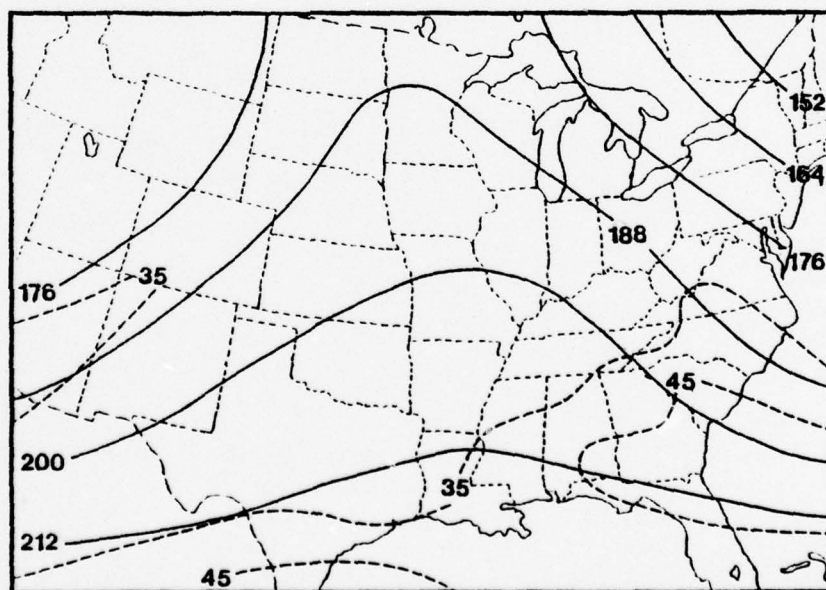


Figure 8 Chart of 200 mb surface for 0000 GMT 14 April 1976; solid lines are contours (gpm) and dashed lines are isotachs ($> 34 \text{ ms}^{-1}$).

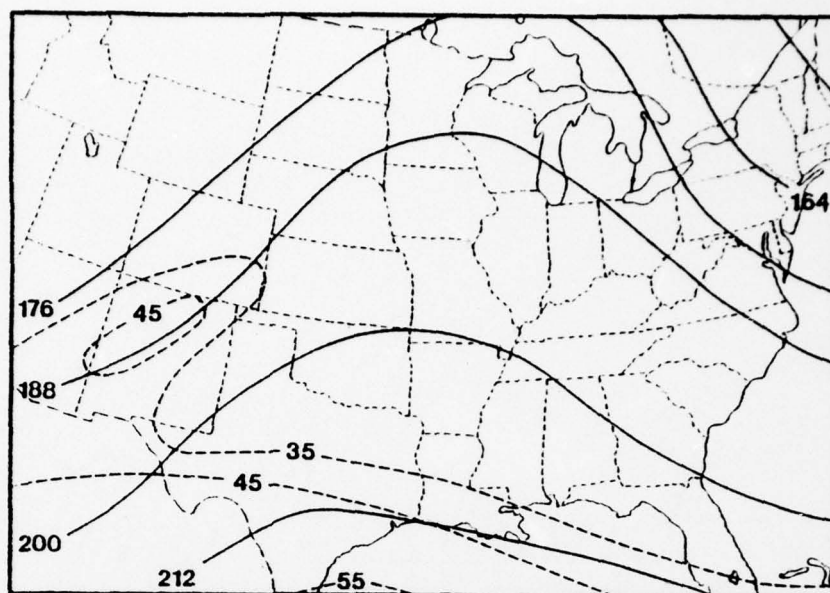


Figure 9 Chart of 200 mb surface for 1200 GMT 14 April 1976; solid lines are contours (gpm) and dashed lines are isotachs ($> 34 \text{ ms}^{-1}$).

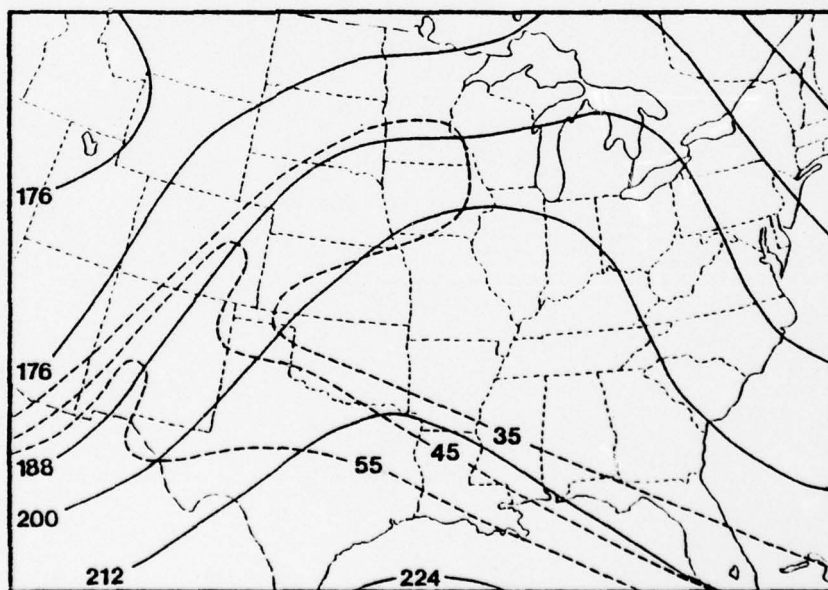


Figure 10 Chart of 200 mb surface for 0000 GMT 15 April 1976; solid lines are contours (gpm) and dashed lines are isotachs ($> 34 \text{ ms}^{-1}$).

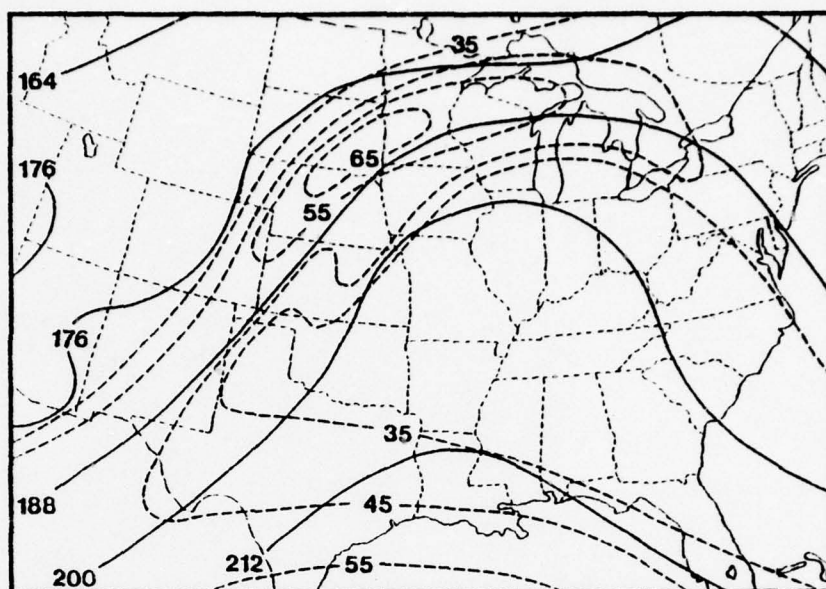


Figure 11 Chart of 200 mb surface for 1200 GMT 15 April 1976; solid lines are contours (gpm) and dashed lines are isotachs ($> 34 \text{ ms}^{-1}$).

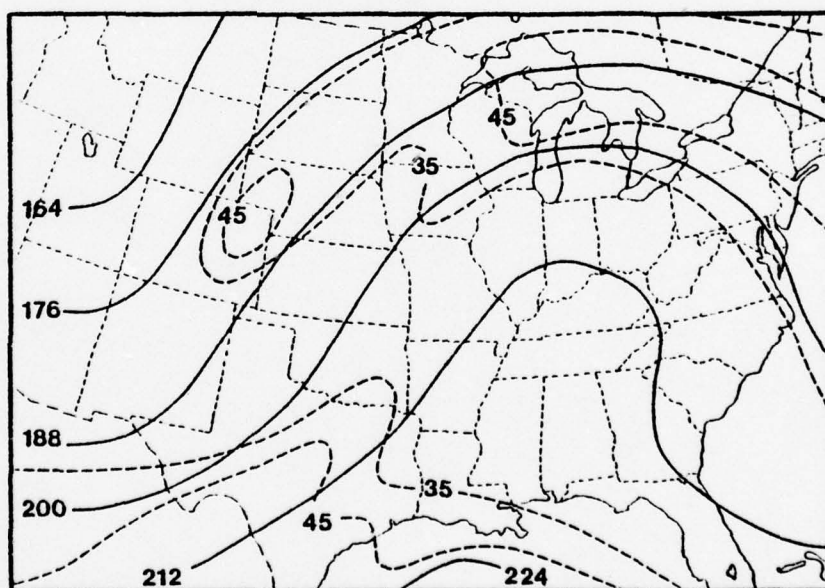


Figure 12 Chart of 200 mb surface for 0000 GMT 16 April 1976; solid lines are contours (gpm) and dashed lines are isotachs ($> 34 \text{ ms}^{-1}$).

By 0000 GMT 14 April wind speeds of 35 ms^{-1} had moved across Oklahoma and northern and western Texas, but still continued over the Southwestern, Southeastern, and Gulf Coast states as shown in Fig. 8. Between 0000 and 1200 GMT 14 April, the area of high wind speeds over the Southwestern states began to separate with the northern branch moving steadily northeastward, while the southern branch moved eastward and merged with the high wind speeds over southern Texas. This resulted in pronounced diffluent flow over the area where severe thunderstorms subsequently developed.

By 1200 GMT 14 April (Fig. 9), the northern branch, with 45 ms^{-1} wind speeds over central New Mexico, was oriented northeast-southwest and extended over the Great Plains. The southern branch, with 55 ms^{-1} wind speeds over southern Texas, was oriented east-west and moved across Mexico and the Gulf Coast states. The area of diffluence covered eastern New Mexico, western and northern Texas, and Oklahoma.

Fig. 10 shows that by the next day the core of maximum wind speeds of the northern branch extended from Mexico across New Mexico, southeastern Colorado, northwestern Kansas into central and eastern Nebraska and northwestern Iowa. Wind speeds of 55 ms^{-1} moved into New Mexico. In the southern branch, 50 ms^{-1} wind speeds now covered most of Texas.

The area of diffluence extended from southeast of El Paso, Texas, across eastern New Mexico, west central Texas and the Texas Panhandle, Oklahoma, Kansas, eastern Nebraska, Iowa, Minnesota, Wisconsin, and Illinois. The significance of this type of motion field in severe weather situations has been described by MacDonald (1977).

During the next twelve hours (0000 to 1200 GMT 15 April), the core of maximum wind speed of the northern branch continued to move northeastward to the Great Lakes, crossed the ridge axis, and began to move southeastward into New York as shown in Fig. 11. This speed core north of the diffluence area produced negative speed shear in addition to the negative curvature over the thunderstorm area. High wind speeds in the southern branch shifted southward with the core center moving from south central Texas to the southern tip of Texas.

On 1200 GMT 15 April, ridging over eastern Canada had separated from the ridging over the eastern U.S., but by 0000 GMT 16 April, the U.S. portion of the ridge was building northward over the Great Lakes and into Canada (Fig. 12). High wind speeds in the northern branch had diminished considerably and moved eastward by this time.

850 Millibar Moisture

Another important synoptic feature that was associated with this severe weather case was the low level moisture field. Southerly flow ahead of the trough began

to advect moisture from the Gulf of Mexico into the Central states in the low levels on 13 April 1976. Figs. 13 to 18 show the 850 mb relative humidity with contours drawn in ten percent increments. A comparison of Figs. 1 and 13 indicates the moisture advection on 13 April 0000 GMT. At this time moist air was present up to 500 mb over parts of Texas and Oklahoma, but during the next twenty-four hours the mid-level moisture advected eastward and was replaced by dry air from the west (relative humidities less than 10 percent) at the 700 and 500 mb levels.

Moist air at 850 mb, which had been in western Texas at 0000 GMT 13 April and moved into the Texas Panhandle by 1200 GMT 13 April, was replaced with dry air by 0000 GMT 14 April (Fig. 14). Between 0000 and 1200 GMT 14 April a slight pressure increase across Texas, coupled with a weakening in the pressure gradient over New Mexico behind the front, increased the low level moisture advection over western Texas (Fig. 15).

Surface temperatures and dew points also increased ahead of the frontal system prior to the outbreak of convective activity. By 1800 GMT 14 April surface temperatures along and ahead of the front in the area of intense thunderstorms, from southwestern Texas to northwestern Iowa, were in the high 70's to low 80's. These temperatures averaged 10°F warmer over Texas, Oklahoma, and

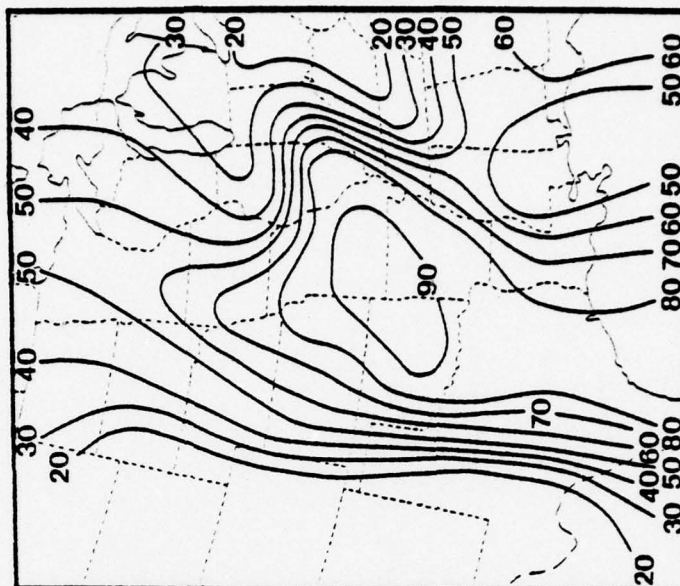


Figure 14 Chart of 850 mb relative humidity for 0000 GMT 14 April 1976; isopleths are in percent.

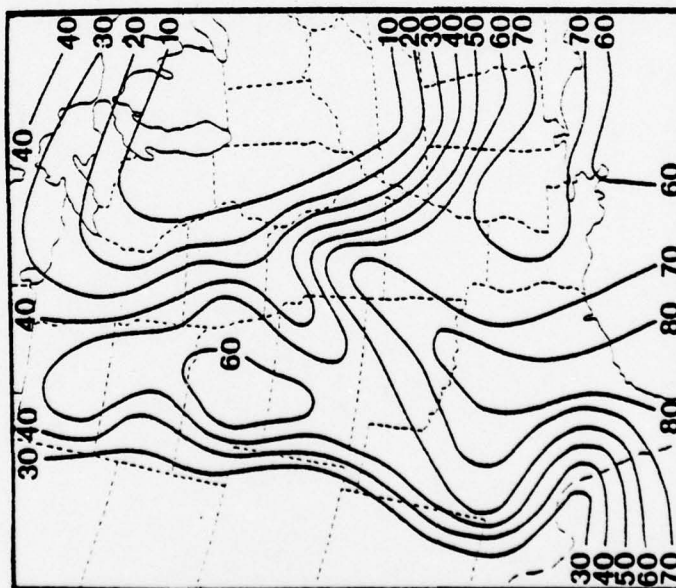


Figure 13 Chart of 850 mb relative humidity for 0000 GMT 13 April 1976; isopleths are in percent.

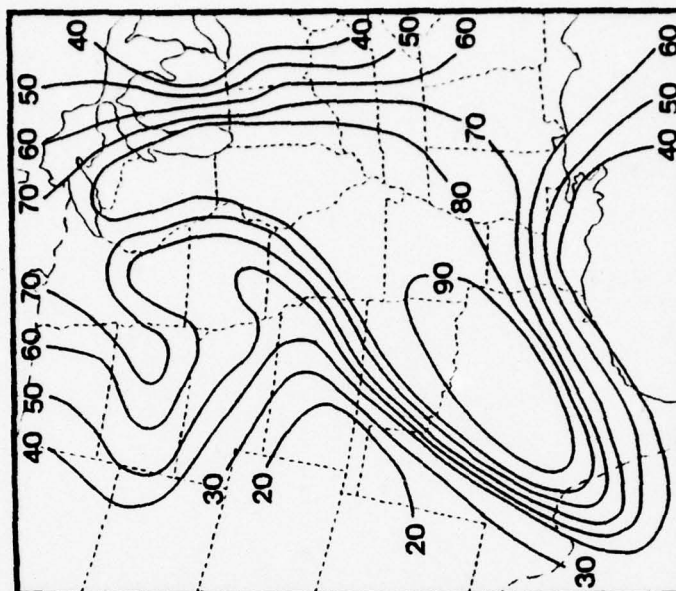


Figure 16 Chart of 850 mb relative humidity for 0000 GMT 15 April 1976; isopleths are in percent.

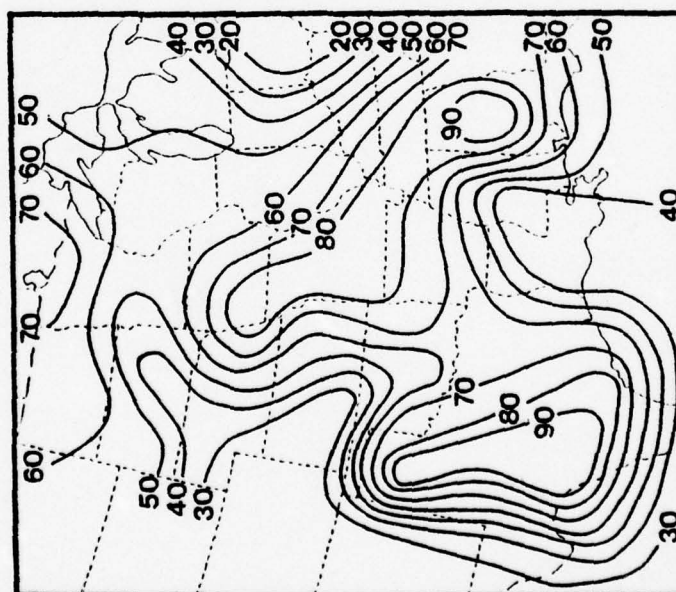


Figure 15 Chart of 850 mb relative humidity for 1200 GMT 14 April 1976; isopleths are in percent.

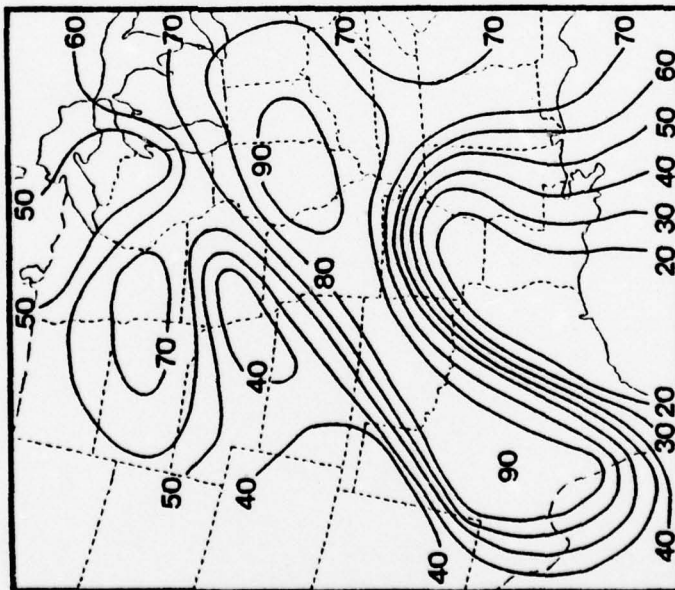


Figure 17 Chart of 850 mb relative humidity for 1200 GMT 15 April 1976; isopleths are in percent.

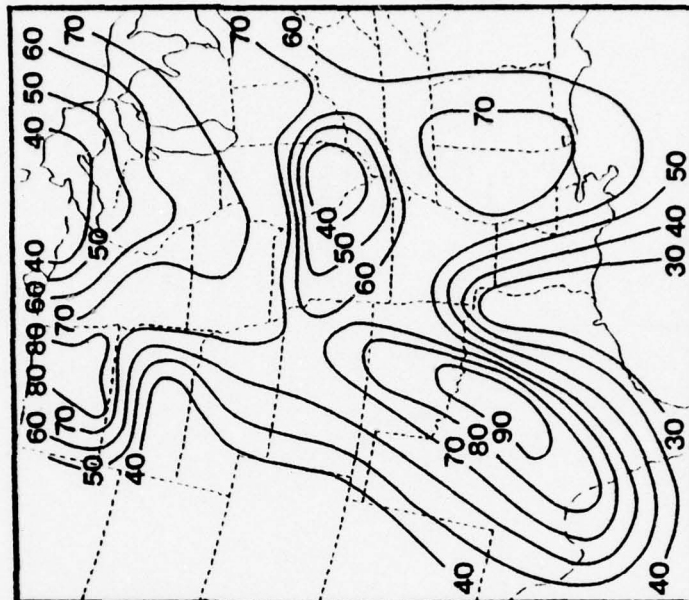


Figure 18 Chart of 850 mb relative humidity for 0000 GMT 16 April 1976; isopleths are in percent.

Kansas, and 5°F warmer over eastern Nebraska and Iowa than in the previous twenty-four hours. The surface dew point temperatures were essentially the same over Texas and Oklahoma for both 1800 GMT reports, 5°F warmer over Kansas and eastern Nebraska, and 10° to 15°F warmer over Iowa. The dew point temperatures decreased rapidly across the front and indicated the presence of a strong moisture gradient. The wind flow ahead of this gradient was moist and southerly; behind the gradient flow was dry and southwesterly. This gradient extended through a deep layer and is depicted at 850 mb in Figs. 15, 16, and 17.

By 0000 GMT 15 April the 850 mb moisture field decreased over western Texas, eastern Kansas, and eastern Nebraska after thunderstorm activity developed throughout these areas. More low level moisture advected into eastern Iowa, Illinois, and Wisconsin (Fig. 16) and provided the moisture source for the thunderstorm activity which moved into southeastern Minnesota and southern Wisconsin during the next twelve hours from Nebraska, Kansas, and Iowa.

Moisture returned to western Texas by 1200 GMT 15 April (Fig. 17) and to the Central Plains states by 0000 GMT 16 April (Fig. 18) as low level southerly flow moved from the Gulf of Mexico into the Central states through this period.

Atmospheric Stability

Figs. 19 through 24 show the Showalter stability index with contours drawn every two units. Fig. 19 displays the values for 0000 GMT 13 April. As of 0035 GMT 13 April, the radar summary indicated that rain showers and thunderstorms were occurring in eastern Colorado, New Mexico, Texas, Oklahoma, and Kansas. This activity initially increased on 13 April, but by 1535 GMT all activity had moved out of these areas.

Generally, the degree of atmospheric stability decreased by 2 to 4 units over the Central states from 0000 GMT 13 April to 0000 GMT 14 April (Fig. 20). Between 0000 GMT and 1200 GMT (Fig. 21) 14 April the stability decreased significantly over western Texas (4 units) while the region of instability over the Central Plain states moved eastward with the front. During this latter period showers and thunderstorms developed over the northern Plains and moved across Minnesota and into northern Wisconsin.

From 1200 GMT 14 April to 0000 GMT 15 April (Fig. 22) instability shifted eastward into central Texas and central Oklahoma and into eastern Iowa, Wisconsin, and Illinois.

No thunderstorm activity was reported in the central and southern Plains states from 1535 GMT 13 April until 1735 GMT 14 April when a single cell with a top of

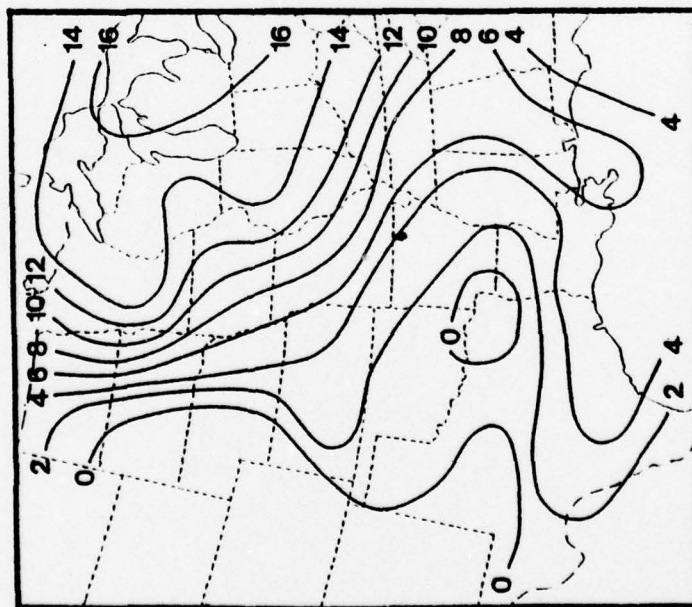


Figure 19 Chart of Showalter stability index for 0000 GMT 13 April 1976.

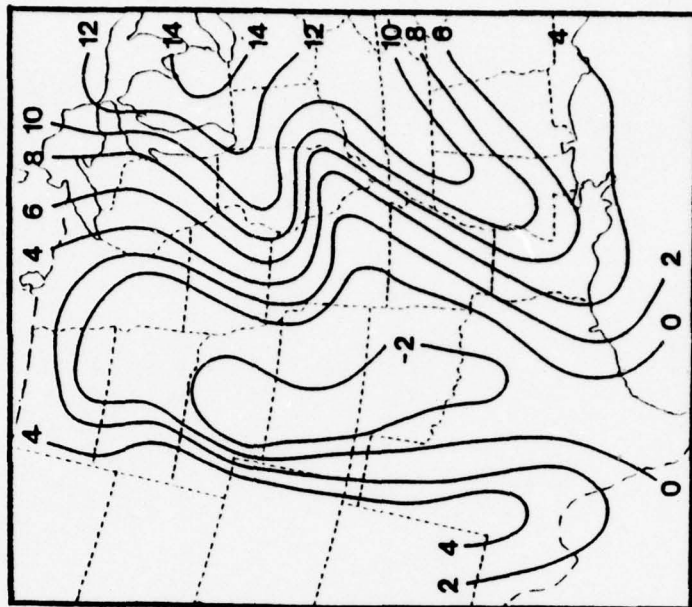


Figure 20 Chart of Showalter stability index for 0000 GMT 14 April 1976.

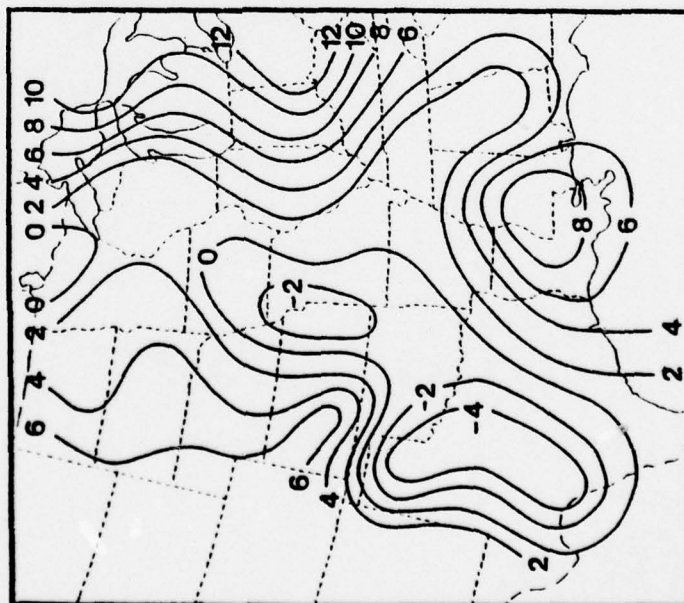


Figure 21 Chart of Showalter stability index for 1200 GMT 14 April 1976.

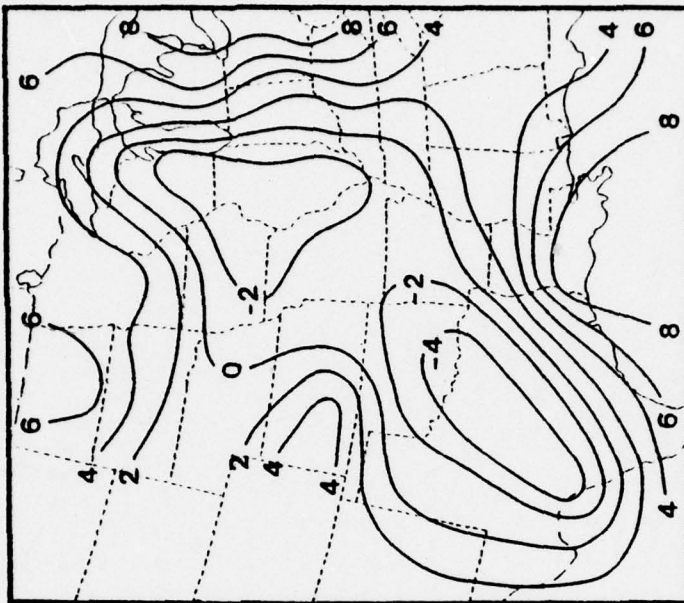


Figure 22 Chart of Showalter stability index for 0000 GMT 15 April 1976.

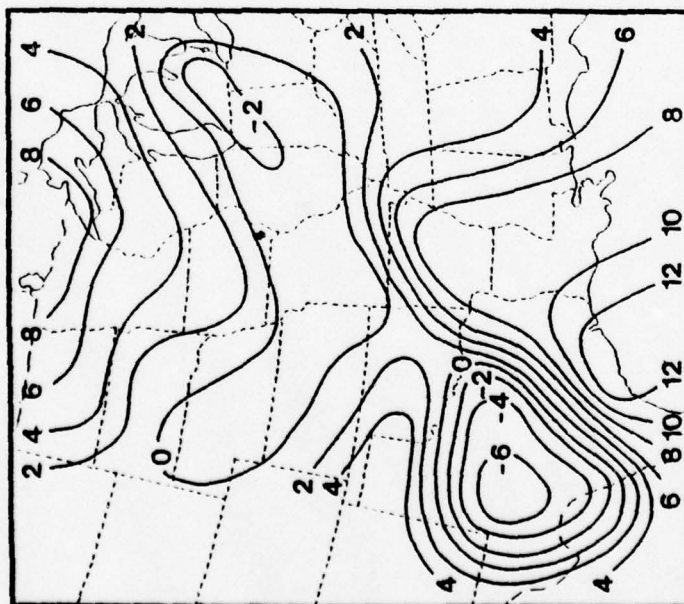


Figure 23 Chart of Showalter stability index for 1200 GMT 15 April 1976.

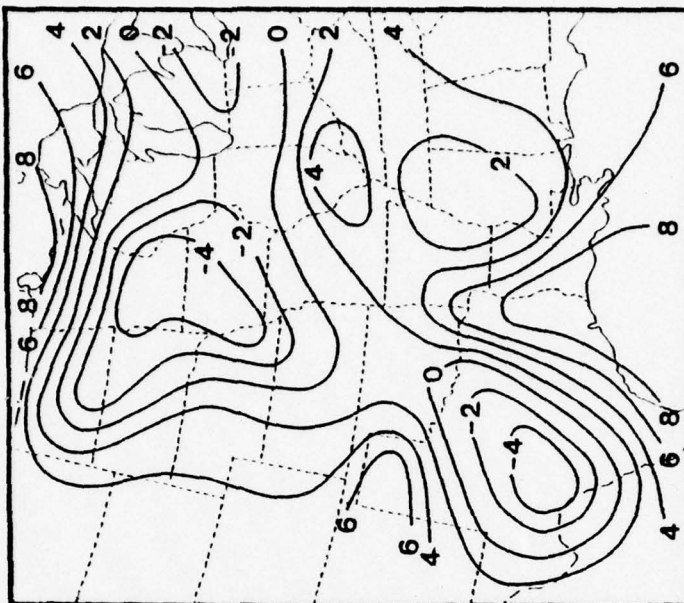


Figure 24 Chart of Showalter stability index for 0000 GMT 16 April 1976.

25,000 ft was observed over southwestern Texas. By 1835 GMT another new cell was reported in the southeastern corner of the Texas Panhandle. Additional cells began developing over New Mexico. At the 1935 GMT radar summary, the cell over the Texas Panhandle dissipated, while many cells formed from El Paso, Texas, northward over the eastern mountains of New Mexico. During these two hours, the original cell slowly intensified and moved northward to extreme southeastern New Mexico. No other activity was reported in the south central Plains; however, during the next hour activity rapidly developed east of the cold front along the low level moisture gradient. By 2035 GMT, thunderstorms with tops of 40,000 ft were reported over central Kansas and south central Nebraska. Thunderstorms with tops to 42,000 ft were reported over extreme southeast New Mexico and western Texas. By 0035 GMT 15 April, lines of activity extended from northeastern Nebraska to south central Kansas and from the Texas Panhandle southward to the Rio Grande River. Tornadoes and 2 to 4 inch diameter hail were reported in Texas, Kansas, and Nebraska near 0035 GMT. During the next nine hours hail, tornadoes, and/or damaging winds continued to be reported in these states and also Iowa and Wisconsin.

Thunderstorm tops in excess of 50,000 ft were reported in all states affected by the severe weather. In several extreme cases, convective tops penetrated the

tropopause by 15,000 ft. Several storms and their tropopause penetrating tops will be discussed in more detail in the next chapter.

Instability areas shifted to southwestern Texas between 0000 GMT 15 April (Fig. 22) and 1200 GMT (Fig. 23) and reappeared over Iowa and Minnesota by 0000 GMT 16 April (Fig. 24). Intense convective activity continued throughout this time period. At 2335 GMT 15 April thunderstorms were reported across western Texas, western Oklahoma, central Kansas, east central Nebraska, Minnesota, North and South Dakota, and Michigan.

CHAPTER III

SATELLITE AND SATELLITE IMAGERY

Satellite

Satellite imagery used in this research was taken by the Geostationary Operational Environmental Satellite (GOES) System. The GOES was in a circular orbit with an altitude of 35,800 km. The spacecraft was controlled for proper earth imaging by an attitude control system in which the spin rate was 100 revolutions per minute. An onboard Visible and Infrared Spin Scan Radiometer (VISSR) provided visual images (0.55 to 0.70 μm band) at 0.8 km (0.43 nm) resolution and infrared images (10.5 to 12.5 μm) at 8 km (4.3 nm) resolution. In a normal scan mode the radiometer scanned from west to east across the earth and provided a full disk image covering nearly one-half of the earth's surface. A full disk image was produced every 30 minutes. Special sectors, called floating sectors, were produced to meet specific requirements such as monitoring severe weather and other rapidly changing meteorological situations. Floating sector images were transmitted more frequently since they covered a smaller geographical area and required

less scanning and processing time. Hence, it was possible to obtain satellite imagery of thunderstorms and other small scale convective systems that were often not resolved by conventional meteorological observations.

Infrared (IR) imagery was enhanced for emphasis of specific features in the imagery. The digital radiance measurements from the satellite were converted to equivalent black body temperatures; then these temperatures were transferred to digital count values. Count values were equated to particular gray shades for television and photographic display purposes. For an IR image, or a nonenhanced image, a linear relationship existed between count value and gray shade. The temperatures displayed in the image change from black shade for the warmest temperatures, through gray, to white for the coldest. By altering this linear relationship, the infrared may be enhanced (enhanced infrared, EIR) to increase the contrast between a particular temperature range and the surrounding temperature field. This alteration was accomplished in two different ways: steep linear enhancement and "step function" enhancement. Steep linear enhancement displays a small count value range, or temperature range, across the gray shades while "step function" enhancement displays a small temperature range at the same gray shade. The steep

linear technique provides excellent detail in the data. The "step function" technique provides contouring in a display thus making deep vertically structured cloud areas obvious.

Satellite imagery in this investigation was enhanced according to Table 1 and corresponded to the enhancement curve illustrated in Fig. 25. Segment 4 through 7 are "step functions" which delineate the vertical structure in convective storms. Segment 8 is a steep linear enhancement, of temperatures -62°C to -80°C , which provides detailed information about the temperature of the storm tops. Segments 2 and 3 give definition to low and middle clouds.

Satellite Imagery

In this thesis, floating sector GOES EIR and IR imagery of a severe weather outbreak over the Central United States on 15 April 1976 was studied. The EIR imagery covered the time period from 0018 GMT to 0947 GMT with images obtained at approximately 15 minute intervals. Fig. 26 shows the EIR image for 0732 GMT. Segments of the enhancement curve (Fig. 25) can be followed from dark gray (lower segment 2) over northern Mississippi to black (segment 7) due west over central Oklahoma. This black shade outlined an elongated area of convective activity which stretched from northern Texas to Lake

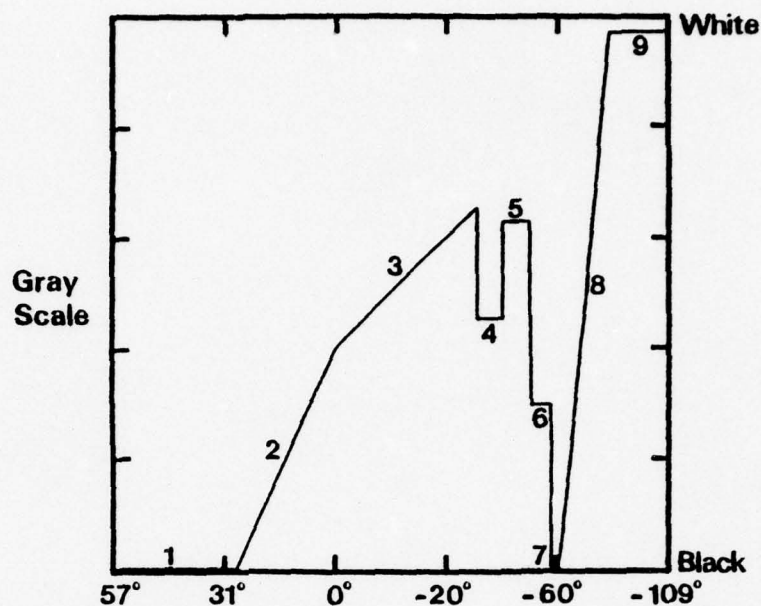


Figure 25 MB enhancement curve for GOES infrared data; abscissa is radiative temperature in $^{\circ}\text{C}$ and ordinate is the image gray scale.

TABLE 1

Relationship between radiative temperature and gray shade in MB type of enhancement for GOES imagery in the 10.5 to 12.5 μm region

Segment Number	Temperature $^{\circ}\text{C}$	Gray Shade
1	$> 28^{\circ}$	black
2	28° to 7°	dark gray
3	7° to -31°	medium gray
4	-31° to -41°	medium gray
5	-41° to -52°	light gray
6	-52° to -58°	dark gray
7	-58° to -62°	black
8	-62° to -80°	black to white
9	$< -80^{\circ}$	white

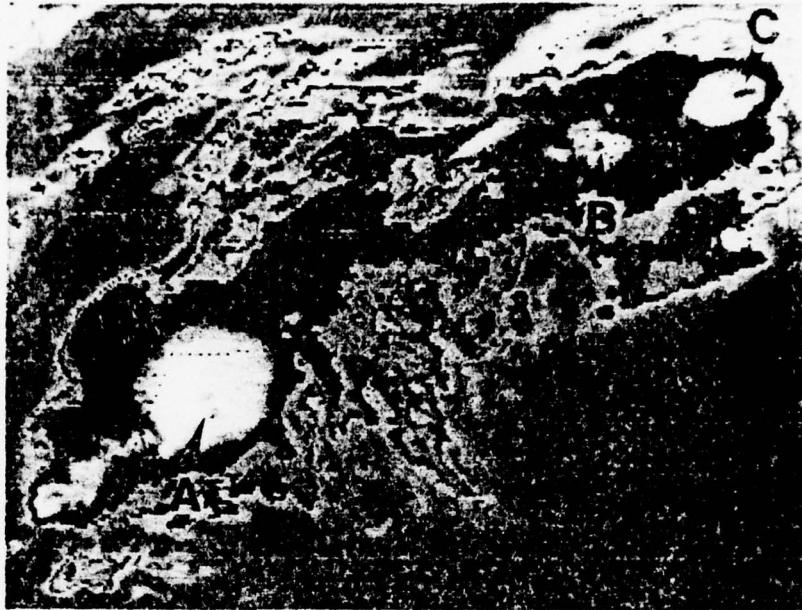


Figure 26 GOES MB enhanced infrared image of the central United States for 0722 GMT 15 April 1976.

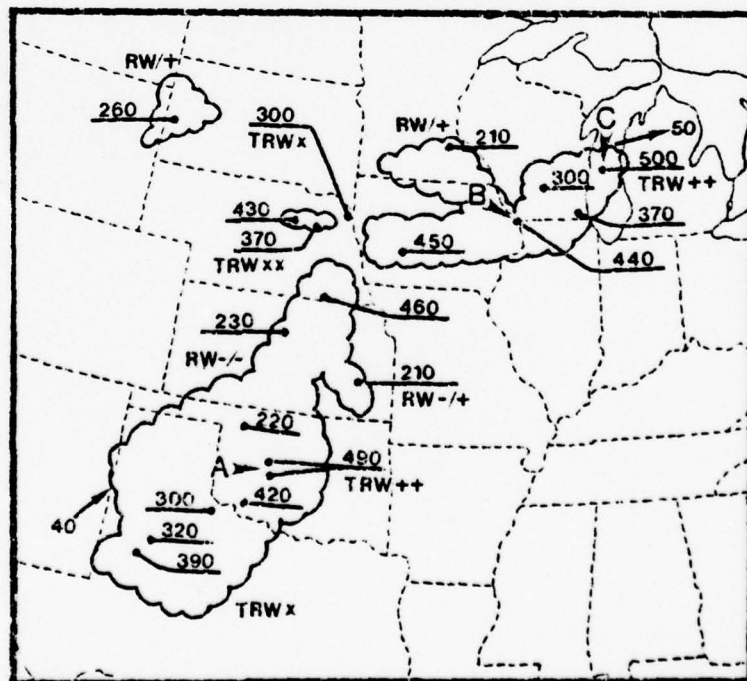


Figure 27 Radar summary of the central United States for 0735 GMT 15 April 1976.

Michigan. This pattern coincided with precipitation echoes shown in the radar summary for 0735 GMT (Fig. 27). The circular shaped white areas within the precipitation region corresponded to the upper portion of segment 8 or segment 9 and depicted the cold radiative temperatures of the convective storm tops.

Temperature information displayed by the segment 8 enhancement was particularly interesting, for imbedded within these circular white areas were gray spots which represented warmer radiative temperatures in the segment 8 temperature range. Furthermore, a comparison of the EIR image and radar summary showed these warm spots were related to very high radar echo tops. The high echo tops have been denoted in Figs. 26 and 27 by points A (two echo tops of 49,000 ft, 14.9 km), B (echo top of 44,000 ft, 13.4 km), and C (echo top of 50,000 ft, 15.2 km).

Fig. 28 shows the EIR image for 0532 GMT and Fig. 29 shows the radar summary for 0535 GMT. A radar echo of 54,000 ft (16.5 km) in extreme eastern Nebraska coincided with a warm spot on the Nebraska-Iowa border. A 50,000 ft (15.2 km) radar top was reported over central Iowa and was related to a warm spot. Also radar echo tops of 54,000 ft (16.5 km) and 57,000 ft (17.4 km) reported over southwestern Wisconsin coincided with an infrared radiative temperature warm spot.



Figure 28 GOES MB enhanced infrared image of Iowa-Wisconsin area for 0532 GMT 15 April 1976.

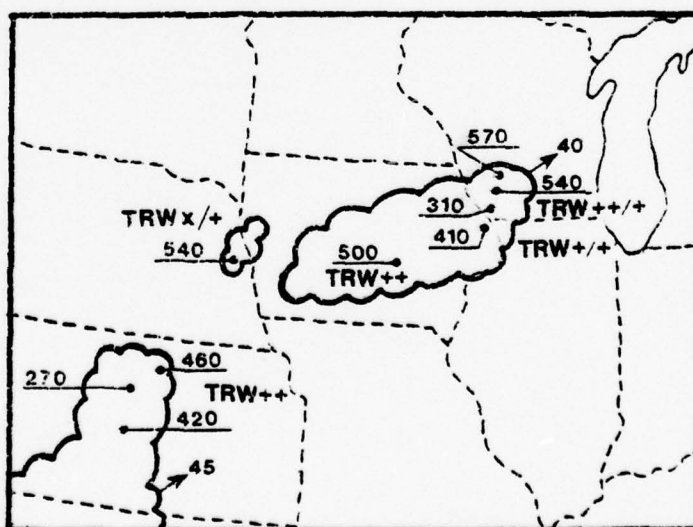


Figure 29 Radar summary of Iowa-Wisconsin area for 0535 GMT 15 April 1976.

Fig. 30 shows the EIR image for 0632 GMT and Fig. 31 shows the radar summary for 0635 GMT. Warm spots appeared over eastern Iowa and central Wisconsin. A 48,000 ft (14.6 km) and 54,000 ft (16.5 km) radar top were reported over central Wisconsin, but no high echo top was reported over eastern Iowa.

Similar features were found on all 33 EIR images from 15 April 0118 GMT to 15 April 0945 GMT. Although radar data was not available at all image times, regular radar observations at 35 minutes past the hour plus occasional special reports on the hour showed almost every warm spot was related to a very high echo top. Every high echo top which was related to a warm spot had penetrated the tropopause, but every high echo top reported to have penetrated the tropopause was not related to a warm spot. Possible explanations for overshooting storm tops producing or not producing warm infrared temperature signatures are discussed in the next chapter.

This investigation also pointed out the importance of the grid size of the GOES EIR image in detecting warm spots as well as the important advantages of GOES EIR imagery over regular IR imagery and over radar observations. For example, Fig. 32 shows the 2330 GMT 14 April 1976 image on a 2 nm grid. Fig. 33 shows the 0130 GMT 15 April image on a 1 nm grid. Although

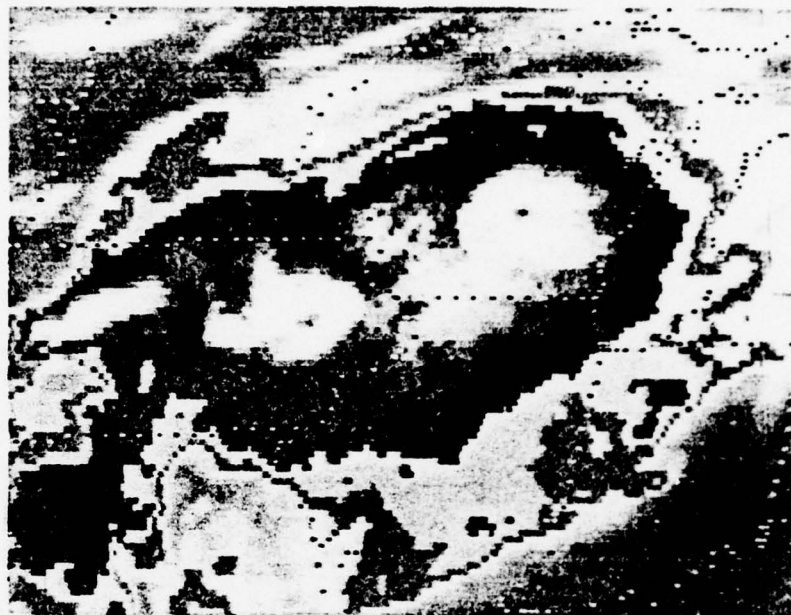


Figure 30 GOES MB enhanced infrared image of Iowa-Wisconsin area for 0632 GMT 15 April 1976.

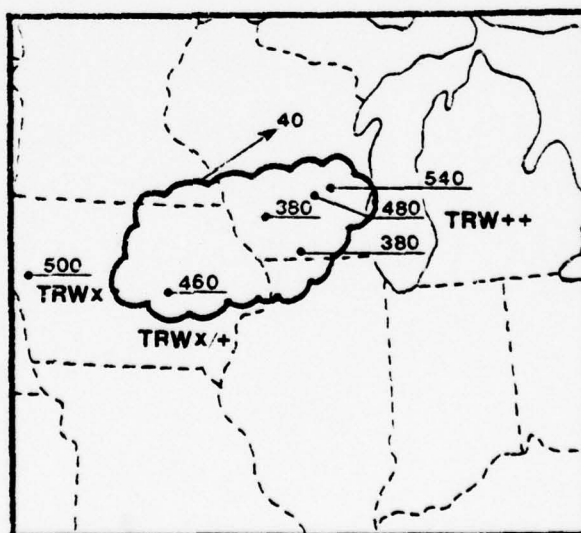


Figure 31 Radar summary of Iowa-Wisconsin area for 0635 GMT 15 April 1976.

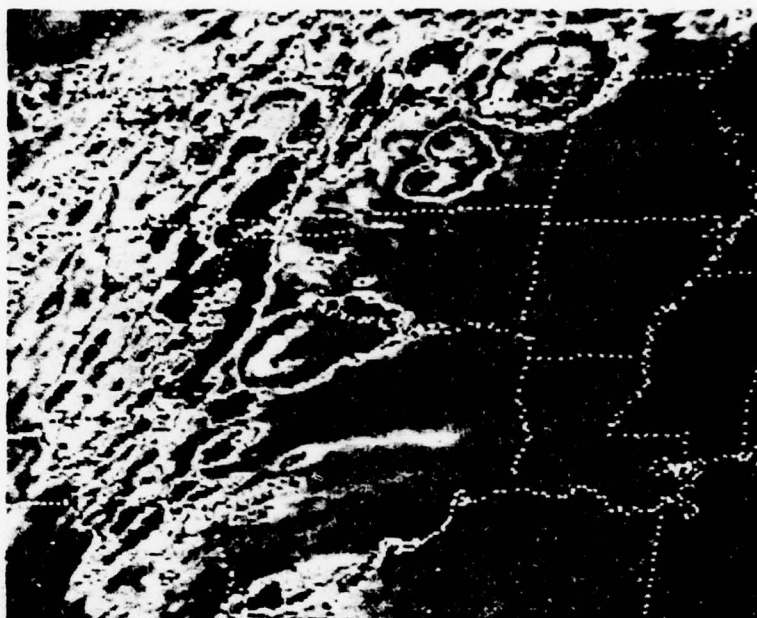


Figure 32 GOES MB enhanced infrared image of central United States for 2330 GMT 14 April 1976; grid 2 nm.



Figure 33 GOES MB enhanced infrared image of central United States for 0130 GMT 15 April 1976; grid 1 nm.

the convective activity has increased from 2330 to 0130 GMT, the sensor resolution in both images is the same and the apparent increased detail was primarily due to the larger gridding.

Fig. 34 shows the IR image for 0730 GMT. The general area of high clouds can easily be seen while exact areas of intense convective activity are not easily discernible. The enhancement of the 0732 GMT EIR image (Fig. 26) clearly delineates areas with coldest radiative temperatures. Although not every white area was associated with intense convective activity, as will be discussed in Chapter IV, the presence of warm spots and the use of conventional radar data helped identify these areas.

Enhanced infrared imagery offers two distinct advantages over radar. One is the short time interval between pictures provided by floating sector imagery. The other is complete coverage of the severe weather area in each image. Together these allowed the forecaster to monitor intense convective activity on a near real time basis, and provided the researcher with unique data to study intense convective development.



Figure 34 GOES infrared image of the central United States for 0730 GMT 15 April 1976.

CHAPTER IV

WARM INFRARED TEMPERATURE SIGNATURES

Warm spots in the GOES EIR imagery appeared to be directly related to tropopause penetrating echo tops. This dependency would give researches and forecasters an additional tool to monitor these high echo tops. In the previous chapter, however, several questions were raised from the comparison of EIR imagery and the radar observations, namely, why do warm spots exist without related high echo tops or vis-a-vis, and what possible explanation for the occurrence of warm spots can be proposed? These questions will be considered in this chapter.

One important characteristic of the warm spots must be considered first. As has already been mentioned, the warm spots appeared as warmer infrared temperatures along the steep linear enhancement of segment 8 (Fig. 25). No black shade of segment 7, separated the warm spot from the surrounding colder radiative temperature area; therefore, the warm spot was part of the cloud whose equivalent black body temperatures lie in the -62°C to -80°C range (segment 8) rather than being associated with clouds of

lower heights and warmer black body temperatures. It is possible that a misinterpretation could occur since several temperature levels in the atmosphere were enhanced with the same gray shade (See Fig. 25).

Warm Spots Without Tropopause Penetrating Tops

The warm spot over central Iowa in Fig. 28, eastern Iowa in Fig. 30, and the Iowa, Illinois, Wisconsin border in Fig. 26 is part of a single storm which can be followed on GOES EIR film loops across central and eastern Iowa from 0502 GMT to 0732 GMT on 15 April 1976. The track of this warm spot extended over a distance of approximately 125 miles as shown in Fig. 35. Its movement corresponded favorably with the movement of high echo tops reported by the WSR-57 radar observations from Des Moines and Marseilles at three different observation times. The two and one-half hour progression of the spot across Iowa suggests the presence of supercell type storms as described by Browning and Foote (1976). These intense quasi-steady state storms exhibit large vertical development over a large horizontal area. Their magnitude is sufficient to account for a 15 to 20 km warm spot imbedded within a 100 km diameter white circular area as observed over central Iowa at 0532 GMT (Fig. 28), eastern Iowa at 0632 GMT (Fig. 30), and eastern Iowa at 0700 GMT (not shown) and 0732 GMT (Fig. 26). Radar observations

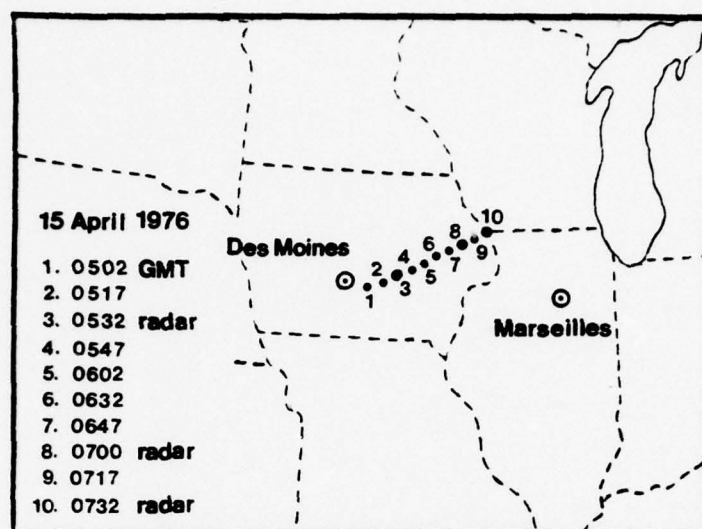


Figure 35 Path of warm spot of MB enhanced infrared images over Iowa from 0502 to 0732 GMT 15 April 1976; corresponding radar positions are shown also.

coincided with the 0532, 0700, and 0732 GMT imagery, but no high echo tops were reported at 0632 GMT. It was concluded that a high echo top was present at 0632 GMT though not observed by radar. Note: the 46,000 ft radar top over Iowa (Fig. 31) was reported by Des Moines slightly southwest of the 50,000 ft radar top reported one hour earlier (Fig. 29). This 46,000 ft convective cell most probably blocked the radar's "view" of the cell associated with the warm spot.

Tropopause penetrating tops without warm spots

Two cases could exist where a tropopause penetrating top would not have an EIR image warm spot. The warm area in the storm top was below the resolution of the GOES IR

sensor (8 km), or the storm top did not have a warm area. An example of this latter case will be discussed in Chapter V.

Explanation of Warm Spots

Surface and rawinsonde data for this synoptic system as well as radar observations were carefully analyzed. These data, together with previous studies of supercell convective storms (*i.e.*, Browning and Foote, 1976; Roach, 1967) were used to formulate three possible explanations to account for the warm spots. These include (1) depressions in the cloud tops, (2) stratospheric cirrus or moisture above the cloud top, and (3) radiative difference and temperature gradients across the cloud top. Each of these factors will now be discussed. Supercell cloud models were developed to explain the warm cloud top temperatures above the strong updraft region and will be presented in the next chapter.

Depressions in the cloud top

The first possible explanation may account for the warm spot if the cloud top collapsed in the adjacent area next to the overshooting updraft. Downward motion associated with a collapsing top would produce a depression in the cloud top and result in a warmer cloud top because of their lower height. Aircraft observations of somewhat smaller convective systems with tops below

40,000 ft (12.3 km) by Fujita (1974) have shown collapsing towers are similar to overshooting turrets in terms of their relatively short duration (less than ten minutes) and small horizontal extent (less than 5 km). This is considerably less than the space and time scales observed in this April 1976 supercell case.

Pitts, Resser, and Mendlowitz (1975), investigating a severe storm over Texas, found significant variations in cloud top equivalent black body temperatures on a 50 m scale and suggested that the measurements could show that each cold anomaly coincided with an overshoot tower and each hot anomaly with a region of subsidence near a tower. This relationship may explain small scale cloud top turrets and subsidence areas, but may not be generalized to explain the warm spots in GOES EIR imagery because of the difference in sensor resolution. For example, the IR sensor reported on by Pitts (1975) observed a spot size of about 45 m on the cloud top. The GOES IR sensor has a resolution of about 8 km. Therefore, the IR and EIR imagery display the large scale radiative temperature pattern smoothing out small scale anomalies. For the tropopause penetrating convective storm tops investigated, the large scale equivalent black body temperature pattern consisted of a 15 to 20 km diameter warm spot, coinciding with the location of the radar reported high echo top,

surrounded by a radiative temperature field approximately 10°C colder.

Additionally, the size and duration of the warm spot shown in Fig. 35, suggests the presence of a quasi-steady mechanism that is characteristic of a supercell storm with very high echo tops as described by Browning and Foote (1976) rather than a pulsating, short lived type of convective system with somewhat lower echo tops as observed by Fujita (1974). For these reasons, a mechanism for maintaining a collapsed anvil top with a circular shape for this 15 April 1976, case would be difficult to explain.

Stratospheric cirrus

Stratospheric cirrus over the central cloud dome may result from a portion of the moist updraft mixing with the stratospheric air and acquiring the warmer ambient temperatures. This has been observed by Umenhofer (1975) as a separate, detached cloud above the convective cloud in other case studies which are not of the supercell type. For example, in order to produce the warm radiative temperatures observed in the Iowa warm spot in Fig. 28 (-70°C), the stratospheric cirrus would have to be very thick and have a high emissivity. Moreover, there would have to be an absence of vertical wind shear above the anvil top so that the cirrus would move at the same speed as the

convective cell and remain circular in shape. In this case, radiosonde data indicated directional shears of more than 20° and speed shears greater than 10 ms^{-1} between the lower stratospheric layers and the radar echo movement. Thus, the second possibility would be as difficult to explain as the depressed anvil top.

Radiative differences and temperature gradients

The third possibility of radiative differences and temperature variations across the cloud top is suggested as a reasonable explanation. This explanation accounts for the large scale EIR features with variations of cloud top parameters and does not rely on physical changes in the cloud itself.

CHAPTER V

CLOUD TOP MODEL

Based on radiosonde observations within the region of convective activity on 15 April 1976, and on studies of radiative properties of cirrus clouds (i.e., Liou, 1974; Kuhn and Weickmann, 1969) a model for a cloud dome of a supercell storm was developed to show how it was possible to have warm cloud top temperatures above a strong updraft region. Fig. 36 shows a vertical cross-section through a cloud dome that is somewhat similar to the visual cloud boundaries of the 21 June 1972 storm that was discussed by Browning and Foote (1976). The main storm top has the appearance of a large, smoothly rounded dome and reached to a height above 15 km. Such a cloud dome is a characteristic feature of vigorous, quasi-steady storms. The updraft region pushes above the tropopause and ascends moist adiabatically to a temperature of approximately -90°C . A pronounced stratospheric inversion exists above the updraft region and consists of small scale mixing as proposed by Roach (1967). The mixing layer is approximately 500 m thick and transports moisture above the layer of coldest temperatures and warms the cloud top by small scale mixing with

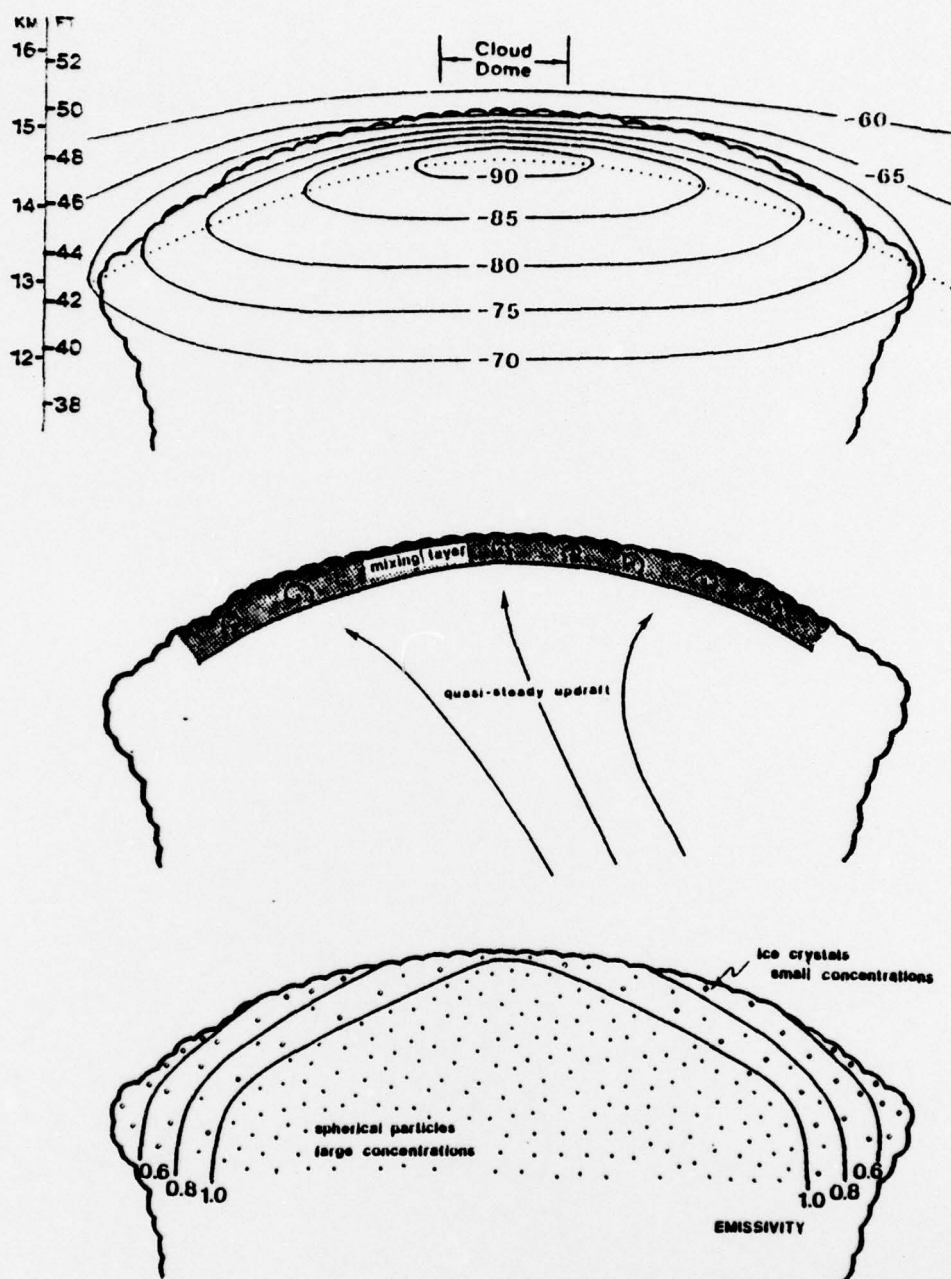


Figure 36 Supercell cloud model with warm cloud dome; temperature, motion fields, and cloud emissivities are depicted.

stratospheric air. Due to weaker ascending motions, the surrounding cirrus anvil does not push as high into the stratosphere. Consequently, cloud top temperatures decrease outward from the central cloud dome.

The lower portion of Fig. 36 schematically represents the cloud particles distribution based on radar observations of supercell storms by Browning and Foote (1976). The strong central updraft region contains relatively large precipitation particles and high concentrations. In contrast the surrounding outer cirrus anvil region is composed of ice crystals and lower concentrations of cloud particles. From several investigations on radiative properties of cirrus clouds by Liou (1974), Kuhn and Weickmann (1969), and Fritz and Rao (1967), it is reasonable to assume that the emissivities at the cloud top would be higher within the updraft region than the surrounding anvil area. Radiation calculations were carried out for this cloud model in order to estimate the effect of emissivity differences across the cloud dome. Emissivity values for the cloud model are schematically depicted in Fig. 36.

Radiation emitted from the cloud top was computed using a multilayer model. This model divided the cloud top into vertical columns 1 km wide. Each column was divided horizontally into layers 250 m thick beginning at the cloud top. Emissivity varied in both the vertical and

horizontal, but within any one 250 m by 1 km layer the emissivity was assumed to be constant.

The upward intensity at the top of each layer, n , was computed from

$$I_{\uparrow}^{\nu}(n) = \epsilon_n B_{\nu}(T_n) + (1 - \epsilon_n) I_{\uparrow}^{\nu}(n + 1) \quad (1)$$

where $I_{\uparrow}^{\nu}(n)$ is the intensity in the 10.5 to 12.5 μm spectral region, ϵ_n is the emissivity of the layer, $B_{\nu}(T_n)$ is the Planck function for the n^{th} layer with average temperature T_n , and $I_{\uparrow}^{\nu}(n + 1)$ is the upward intensity from the layer below.

The upward intensity at the top of the cloud was assumed to equal the infrared emission measured by the satellite. This radiance measurement was converted to an equivalent black body temperature and then was compared to the enhancement curve (Fig. 25). The purpose was to see if the calculated cloud top temperature field would give the same gray shade pattern as observed in the GOES EIR imagery.

Fig. 37 illustrates the results of computations using Eq. 1. This diagram displays the temperature difference between the cloud top dome and cloud top at various radial distances from the dome. A simple two layer model with the lower layer ten degrees colder was used. Curve 'a' represents the radial temperature variation when emissivity was unity across the entire cloud top.

This curve accounts for only a 5°C difference between the cloud dome and the cloud top a radial distance R_3 from the dome. When emissivity was allowed to decrease according to the values shown along the top of Fig. 37, then a larger radial temperature gradient of 8°C was calculated and was depicted as curve 'b'. Curves 'c' and 'd' correspond to 'a' and 'b' except the cloud dome was specified as being colder than the surrounding cirrus anvil.

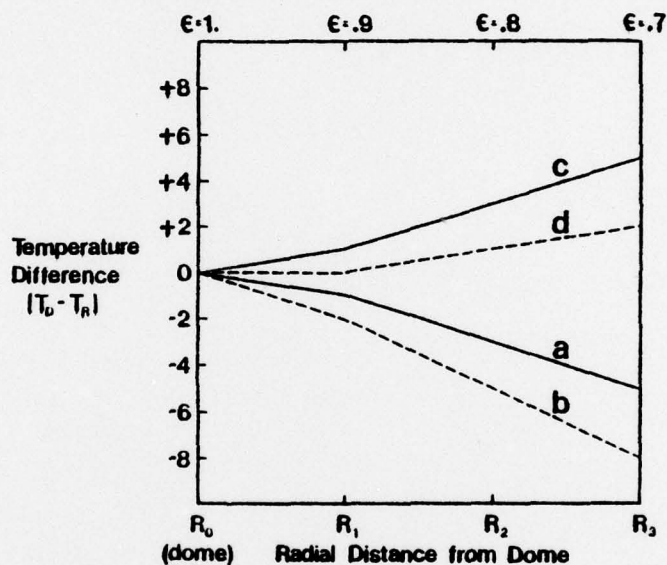


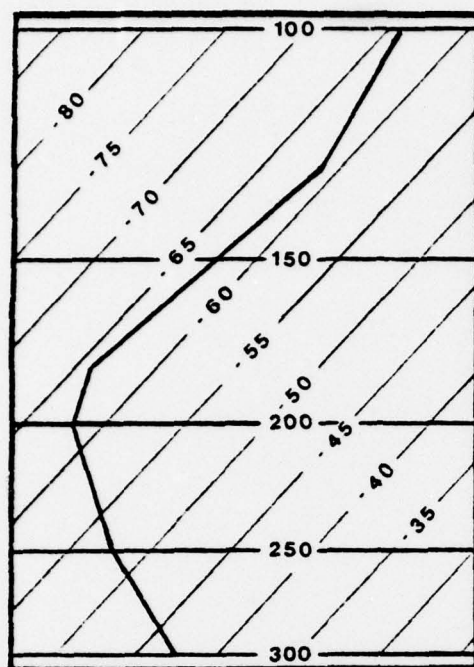
Figure 37 Infrared radiative temperature difference between the central cloud dome and various radial distances from the dome.

These simple calculations illustrate the significance of variations in the emissivity and temperature across the cloud top. Temperature variation alone, with emissivity of unity, could explain the warm spot over

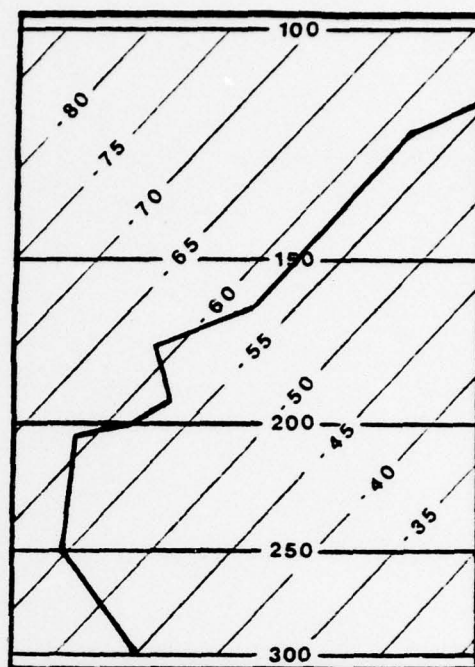
central Iowa in Fig. 28, but warm spots were also observed for radar echoes of 44,000 ft (13.4 km) and 46,000 ft (14 km), and the outer edge of these cloud tops would require temperatures colder than moist adiabatic ascent temperatures in order to explain the EIR imagery.

The radar summary for 0535 GMT (Fig. 29) also showed an area of convective activity over a portion of northeastern Iowa; however, no significant echo tops were reported. The coldest temperatures at the radiosonde stations for Oklahoma City and St. Cloud at 0000 GMT and 1200 GMT 15 April were -71°C (see Fig. 38) while the corresponding satellite image indicated -80°C cloud top radiative temperatures. Therefore, emissivity values less than unity must have existed in order to explain the extensive area of -80°C infrared radiative temperatures. Since low emissivity values were present in this area, then it was reasonable to assume that low values were present in adjacent convective cloud tops in Fig. 28 and other EIR imagery.

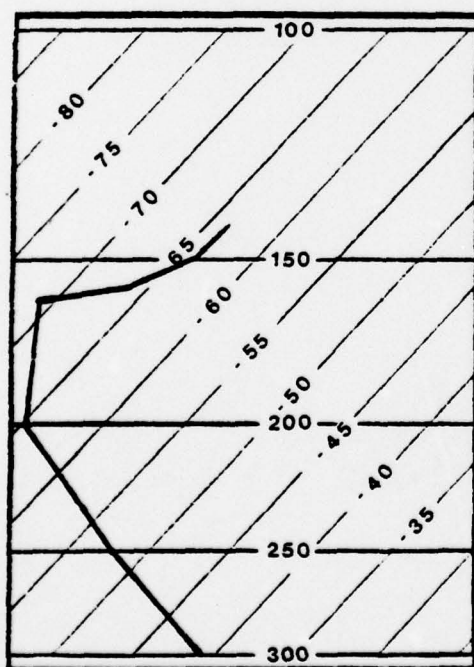
An attempt was made to duplicate the temperature profile shown in the GOES EIR image for the cloud top over central Iowa in Fig. 28. The model cloud top (Fig. 36) was divided into four concentric circular areas depicted in Fig. 39. Cloud top upward intensities were calculated from Eq. 1 for each column within the circular area, averaged, and converted to an equivalent black



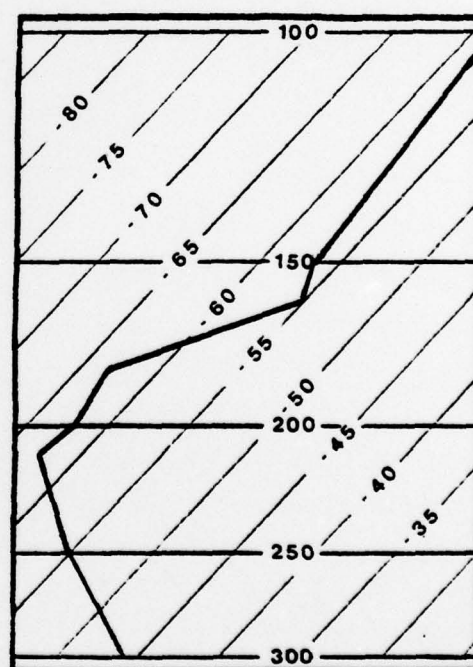
0000 GMT



0000 GMT



1200 GMT



1200 GMT

Figure 38 Radiosonde data for Oklahoma City (left) and St. Cloud (right) 15 April 1976.

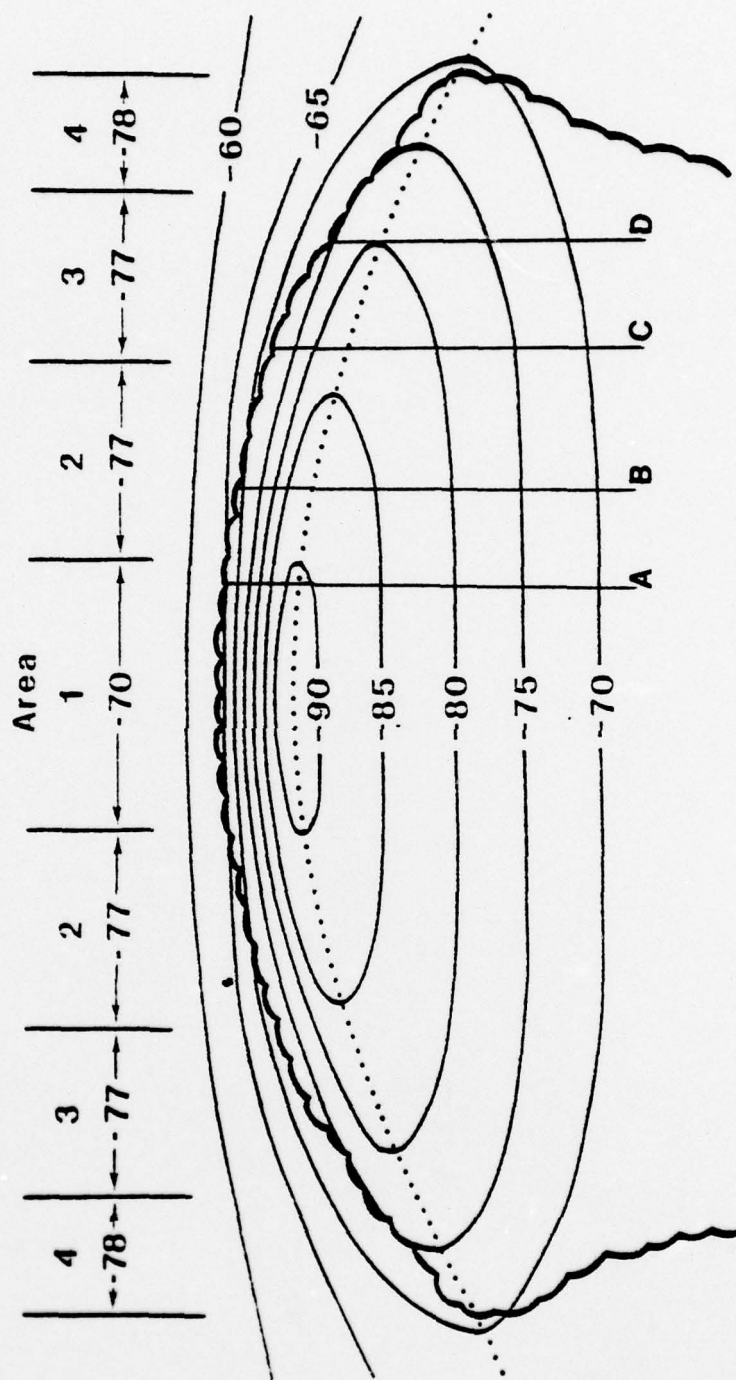


Figure 39 Cloud dome model for central Iowa warm spot shown in Fig. 28; vertical lines A, B, C, and D represent selected columns the temperature, emissivity, and equivalent black body temperature of which are shown in Table 2.

body temperature. The results are displayed in Fig. 39. Table 2 shows the layer temperature and emissivity values used for selected columns (layer 1 is at the cloud top), and the equivalent black body temperature for that column. The column identifier corresponds to a vertical line with the same letter in Fig. 39. There is reasonable agreement between the model calculations and the satellite imagery.

As discussed in Chapter IV, some radar reported tropopause penetrating convective storms were not associated with warm spot infrared signatures on the GOES EIR image. For 15 April 1976 cases, the warm area was below the resolution of the infrared sensor, or the activity may not have been in the stratosphere long enough to develop a warm area. On other days, the stratospheric inversion may be very weak and no significant temperature gradient will develop across the cloud top. Fig. 40 shows an example of a convective dome that was associated with a weak stratospheric inversion. Under this condition the cloud dome would be cold relative to the surrounding cirrus anvil.

TABLE 2

Temperature and emissivity values used in radiative transfer calculations for four selected columns in Fig. 38. Equivalent black body temperature for each column is shown also.

Column in Fig. 38	Equivalent Black Body Temperature	Layers																	
		1	2	3	4	5	6	7	8	9									
		T°C	ε	T°C	ε	T°C	ε	T°C	ε	T°C	ε	T°C	ε	T°C	ε	T°C	ε	T°C	ε
A	-70°C	-70	.95	-78	1.0	-85	1.0	-89	1.0	-87	1.0	-85	1.0	-83	1.0	-81	1.0	-79	1.0
B	-77°C	-76	.85	-85	.90	-86	.95	-85	1.0	-83	1.0	-81	1.0	-79	1.0	-77	1.0	-75	1.0
C	-77°C	-76	.70	-81	.75	-82	.80	-80	.85	-78	.90	-76	.95	-74	1.0	-72	1.0	-70	1.0
D	-77°C	-76	.60	-78	.65	-77	.70	-76	.75	-74	.80	-72	.85	-70	.90	-68	.95	-66	1.0

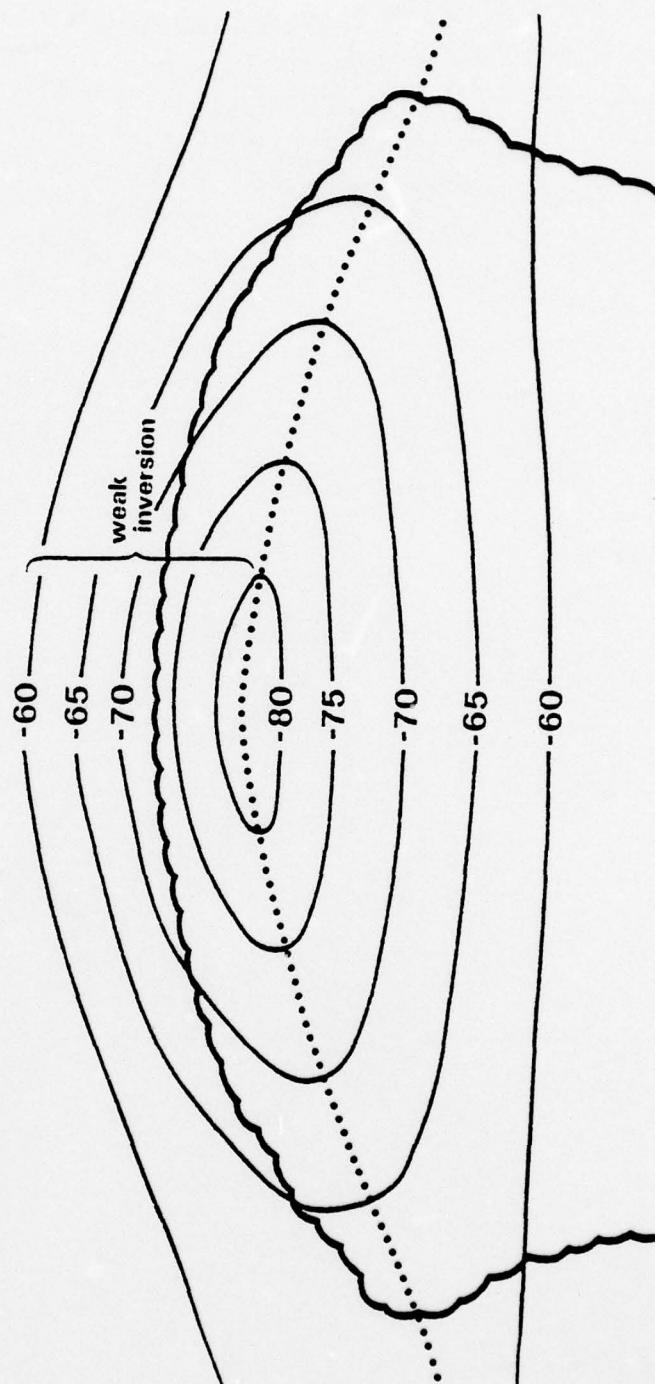


Figure 40 Model of a supercell with a cold cloud dome.

CHAPTER VI

SUMMARY AND FURTHER STUDIES

GOES enhanced infrared images provided detailed information about radiative temperature patterns of cirrus anvil tops associated with a local severe storm situation for 15 April 1976. Warm infrared radiative temperature areas imbedded within cold cirrus anvil domes corresponded to radar echoes that penetrated the tropopause. A cloud top model was presented to attempt to explain the correspondence for this case. Horizontal and vertical temperature gradients at the cloud top together with emissivity differences can explain the warm spot radiative temperature signature.

It is not known how often this phenomenon may be observed because enhanced infrared imagery is a relatively new tool for use in the analysis and forecasting of convective cloud systems. There are a number of different types of convective systems that may produce EIR signatures similar to the one discussed here and this cloud top model is not applicable to all cases. Further research on this problem is needed, especially, as man-interactive image and data processing systems are developed for operational analyses.

REFERENCES

- Browning, K.A., and G.B. Foote, 1976: Airflow and hail growth in supercell storms and some implications for hail suppression, Quarterly Journal of the Royal Meteorological Society, 102, 499-533.
- Corbell, R.P., C.J. Callanan, and W.J. Kotsch, Editors, 1977: The GOES/SMS User's Guide, NOAA/NASA Publication, Washington, D.C., 118 pp.
- Fritz, S., and P.K. Rao, 1967: On the infrared transmission through cirrus clouds and the estimation of relative humidity, Journal of Applied Meteorology, 6, 1088-1096.
- Fujita, T.T., 1974: Overshooting thunderheads observed from ATS and Learjet, Report No. 117, Satellite and Meso-meteorology Research Project, Department of Geophysical Sciences, University of Chicago, 29 pp.
- Kuhn, P.M., and H.K. Weickmann, 1969: High-altitude radiometric measurements of cirrus, Journal of Applied Meteorology, 8, 147-154.
- Liou, K.N., 1974: On the radiative properties of cirrus in the window region and their influence on remote sensing of the atmosphere, Journal of the Atmospheric Sciences, 31, 522-532.
- MacDonald, A.E., 1977: On a type of strongly divergent steady state, Monthly Weather Review, 105, 771-785.
- Martin, D.W., 1975: Characteristics of West African and Atlantic cloud clusters, Preliminary Scientific Results, Vol. 1, GATE Report No. 14, GARP, ICSU, WMO, 182-190.
- Mills, P.B., and E.G. Rutling, 1977: Detection of tropopause penetrations by intense convection with GOES enhanced infrared imagery, Preprint Volume, Tenth Conference on Severe Local Storms, Omaha, Nebraska, 61-64.

- Pitts, D.E., W.K. Reeser, and M.A. Mendlowitz, 1975: Equivalent blackbody temperature of the top of a severe storm, Journal of Applied Meteorology, 14, 609-618.
- Roach, W.T., 1967: On the nature of the summit areas of severe storms in Oklahoma, Quarterly Journal of the Royal Meteorological Society, 93, 318-336.
- Umenhofer, T.A., 1976: Overshooting top behavior of three tornado producing thunderstorms, Preprint Volume, Ninth Conference on Severe Local Storms, Norman, Oklahoma, 96-99.

VITA

Name	Peter Benton Mills
Birthplace	Dayton, Ohio
Birthdate	March 1, 1942
High School	Fairmont High School Kettering, Ohio
Universities	Purdue University
1960-1962	West Lafayette, Indiana
1962-1963	Pennsylvania State University University Park, Pennsylvania
1963-1966	Ohio State University Columbus, Ohio
1969-1970	University of Utah
1976-1978	Salt Lake City, Utah
Degree	B.S., University of Utah
1970	Salt Lake City, Utah
Honorary Societies	Chi Epsilon Pi
Professional Position	Weather Officer United States Air Force